Identifying and targeting cancer-specific metabolism with network-based drug target prediction
Supplementary text, tables, and figures

Maria Pires Pacheco[1], Tamara Bintener[1], Dominik Ternes[1], Dagmar Kulms[2,3], Serge Haan[1], Elisabeth Letellier[1], Thomas Sauter[1*]

Abstract
Background: Metabolic rewiring allows cancer cells to sustain high proliferation rates. Thus, targeting only the cancer-specific cellular metabolism will safeguard healthy tissues.
Methods: We developed the very efficient FASTCORMICS RNA-seq workflow (rFASTCORMICS) to build 10 005 high-resolution metabolic models from the TCGA dataset to capture metabolic rewiring strategies in cancer cells. Colorectal cancer (CRC) was used as a test case for a repurposing workflow based on rFASTCORMICS.
Findings: Alternative pathways that are not required for proliferation or survival tend to be shut down and, therefore, tumours display cancer-specific essential genes that are significantly enriched for known drug targets. We identified naftifine, ketoconazole, and mimosine as new potential CRC drugs, which were experimentally validated.
Interpretation: The here presented rFASTCORMICS workflow successfully reconstructs a metabolic model based on RNA-seq data and successfully predicted drug targets and drugs not yet indicted for colorectal cancer.
Funding: This study was supported by the University of Luxembourg (IRP grant scheme; R-AGR-0755-12), the Luxembourg National Research Fund (FNR PRIDE PRIDE15/10675146/CANBIO), the Fondation Cancer (Luxembourg), the European Union's Horizon2020 research and innovation programme under the Marie Sklodowska- Curie grant agreement No 642295 (MEL-PLEX), and the German Federal Ministry of Education and Research (BMBF) within the project MelanomSensitivity (BMBF/BM/7643621).

Keywords
Metabolic modelling — Cancer — Machine learning — Drug Repurposing

[1] *Life Sciences Research Unit, University of Luxembourg, Esch-Alzette, Luxembourg*
[2] *Experimental Dermatology, Department of Dermatology, Technical University Dresden, Dresden, Germany*
[3] *Center for Regenerative Therapies, Technical University Dresden, Dresden, Germany*
*__Corresponding author__: Thomas Sauter, Systems Biology Group, University of Luxembourg, Luxembourg
E-mail adress: thomas.sauter@uni.lu

1. Supplementary text, tables, and figures

2. Supplementary Text

2.1 Similarity testing

rFASTCORMICS captures metabolic variations between the cancerous and the control models. We found that, for the discretized data (the preprocessing step of rFASTCORMICS), the samples cluster according to their tissue-type (see Figure S.2). This behaviour is also observed for the models that were reconstructed from the same tissue. They cluster together, regardless of their healthy state (see Figure S.3). However, when each model from a tissue is considered separately, a clear clustering between cancer and control is observed. Cancerous samples are less homogeneous than their healthy counterparts (see Figure S.4, S.5, and S.8). See Table S.1 for the abbreviations of the tissues.

2.2 Signatures

2.2.1 Reaction signatures

To further assess the capability of rFASTCORMICS to capture metabolic alterations and to verify if alterations are part of a strategic rewiring, a feature selection approach was used to find cancer and control-specific reactions and genes (see Figure S.9).

Reaction signatures were retrieved using a reverse selection approach for all 13 tissues. The reaction signatures contained between 12 and 100 reactions for each tested tissue (total of 583 reactions) and the prediction accuracy was above 94% (see Figure S.10). In total, among the reaction signatures, 346 out of 583 reactions were more frequently found to be active in the control than in the cancer models. 175 were more often found to be active in at least one cancer type. 62 reactions were found to be more active in a least one cancer type and more often inactive in another. Most reactions could only be found in one signature but MM6ag was present in 5 different signatures. MM6ag is under the control of MAN1C1 (mannosidase alpha class 1C member 1) and is a potential hepatocarcinoma biomarker.[1]

In hepatocarcinoma, several branches of pathways consuming building blocks such as amino acids, nucleotides, nucleotides are shut-down. Additionally, a sub-branch of the N-glycan synthesis pathway was present in 78% of the hepatocarcinoma models against only 36% of the healthy liver models (see Figure S.11).

Overall, among the reaction signatures, the fraction of active reactions per pathway is smaller in the cancer models. Pathways that are downregulated in cancer include the biotin pathway (COAD, LUAD, LUSC, STAD), phenylalanine synthesis (KICH, LUSC), and the heme pathway (BRCA), indicating metabolic rewiring strategies (see Figure S.12). For COAD tumour cells, reactions from keratan sulfate, o-glycan, glycerophospholipid and sphingolipid lipids were less often active in cancer cells, whereas a higher faction of blood group synthesis was more often active in the cancer samples (LUAD, THCA).

2.2.2 Genes signatures

A similar approach was used to obtain gene signatures that are able to predict the label of a sample (cancerous or control) with an accuracy above 95% (see Figure S.13). The gene signatures are more often active in the control than in the cancer samples: 305 out of 502 genes were more often inactive in at least one cancer type. 147 genes were active in at least one cancer type and inactive in controls, whereas 49 genes were more often active in one cancer type than the controls but more inactive in another.

To validate the gene signatures, we searched for enrichments in known cancer driver genes, functional (and truncating) mutations, as well as homozygous deletions. Again, a strong enrichment against metabolic genes has been found (p-values between 0.02 and 0.0002, see Figure S.14)

Gene that code for transporters have been shown to play a crucial role in the activation of metabolic pathways in macrophages and to be under high-regulatory load.[2] Therefore, the gene signatures were tested for solute carriers and ATP-binding cassette (ABC) transporters. Results show a strong enrichment for both transporter types compared to the metabolic genes (p-values = 1.5 10e-8 and 0.0209 for solute carriers and ABC transporters, respectively, see Figure S.14 and Figure S.15).

Among the solute carriers, 65 were more often present in cancer cells, 28 in the controls and 7 were tissue dependent. Further, two solute carriers were found in 3 gene signatures: SLC12A1 and SLC28A3 were more often found in cancer and control samples, respectively.

To confirm if possible mutations in the gene signatures are associated to different phenotypes, results from somatic mutation prediction algorithms such as MUSE,[3] MUTECT2,[4] sniper,[5] and VarScan2[6] were compared to the gene signatures. The outcome revealed enrichments (hypergeometric test: p-values between 0.0027 and 2.3 10e-5, see Figure S.14 and Figure S.15) and suggests that mutations in 97% of the genes in the signature have a high phenotypic impact when compared to the metabolic genes, but the number of mutations varies among the different tissues.

Significant enrichments were also found for each tissue and algorithm combination (except for KICH and MUSE). Metabolic genes are less enriched for high-impact mutations than genes in the signatures but are nevertheless enriched when compared to non-metabolic genes. For 8 of the 13 tissues and for 3 of the 4 algorithms, the enrichment was significant for metabolic genes when compared to non-metabolic genes (looking at each tissue individually) there was a strong enrichment when the tissues were pooled (see Figure S.16). Further inspection of the gene signatures revealed 21 super-enhancers, which are hypo-methylated in colon cancer, glioblastoma, small cell, and non-small cell lung cancer (p-value 0.0038).

To further validate the results from the gene signatures, we referred to the literature. ADH1B, which is known to synergistically enhance the risk of oesophageal,[7,8] bladder,[9] and head and neck cancer,[10] was found in the gene signatures of 10 tissues. Similarly, CA4 was found in 6 out of 13 tissues and a significant correlation between different alleles

of these genes and an increase or a decrease of colon cancer risk[11,12] was shown for the male[13] population especially in the south-western Chinese population.[14]

Further inspection of the gene signatures revealed 21 super-enhancers, which are hypo-methylated in colon cancer, glioblastoma, small cell, and non-small cell lung cancer (p-value 0.0038).

Lastly, the gene and reaction signatures as well as the predicted essential genes are coherent with the previous knowledge as shown by the enrichment tests and literature search. For example, heme oxygenase 1 was shown to inhibit breast cancer invasion[15] and modifications in the glycosylation processes are well described in cancer and are known to be hallmarks of cancer progression.[16] Further, biotin plays a key role in DNA repair and in the regulation of gene expression, particularly of oncogenes in small cell lung cancer.[17] PYCR1, present in numerous signatures, is overexpressed in cancer cells, notably in the metastasis of prostate cancer[18] and was shown to act as an anti-cancer suppressor in breast cancer when knocked-down.[19]

2.3 Cancer models and cancer core metabolism are more compact

Cancer models are smaller than the control models (see Figure S.6, Figure S.5, and Table S.2). There are more common reactions and genes in the controls models compared to the same number of cancer models (Figure S.17 and S.18, respectively). The smaller size of the cancer core metabolism is accompanied by an enrichment of essential genes (Figure S.19) and is caused by a shut down of alternative pathways that are not required for survival (see Figure S.20, Figure S.21, Figure S.22, and Table S.4). Essential genes were shown to have higher expression values and, as the cancer core metabolism is enriched for essential genes, genes in the cancer core have higher expression values (see Figure S.23).

2.4 Essential gene and drug prediction

The reconstructed generic metabolic models were used to predict cancer-specific essential genes (for the workflow, see Figure S.24). The DrugBank database was datamined to find drugs that target these essential genes. Growth rates based on the biomass and ATP production are given in Figures S.25, Figure S.26, Figure S.27, and Table S.5. The predicted essential genes are enriched for essential genes identified by CRISPR technology in cancer cell lines (Figure S.28). Three drugs, namely ketoconazole, naftifine and mimosine (see Table S.7) were validated on T6 cells, HT29 cells and Caco-2 cells (see Figure S.30).

2.5 Comparison to the INIT algorithm

In order to assess the prediction power of a different model reconstruction algorithms, we used INIT[20] to reconstruct 13 generic cancer and 13 generic control models from the TCGA dataset. Only tissues with a minimum of 13 control samples were considered. For each cancer and control model, 25 random samples of the condition and tissue were selected. The INIT algorithm was implemented in the COBRA toolbox and needs an input model to extract the context-specific model from and an array of weights where each row corresponds to a reaction in the input model (here: the consistent Recon 2 model). The weights can be positive or negative depending on the reaction presence. To avoid the effect of an arbitrary threshold, the FPKM values were discretized using the rFASTCORMICS workflow, and each discretized gene was mapped to the reactions of the input model using the GPR rules. Based on the discretization, we obtained a matrix of weights in which each column corresponds to one of the 25 random samples for a condition and each row corresponds to a reaction. In order to create one generic model, a reactions was considered to be active (1) if it is active at least 90% of the samples and inactive (-1) if it is inactive in at least 90% of the samples. If neither active not inactive state could be associated, 0 was taken as weights for that reaction. Both the ATP demand and biomass reaction were forced to be included by assigning their reactions a weight of 10.

3. Supplementary Figures

3.1 Model analysis

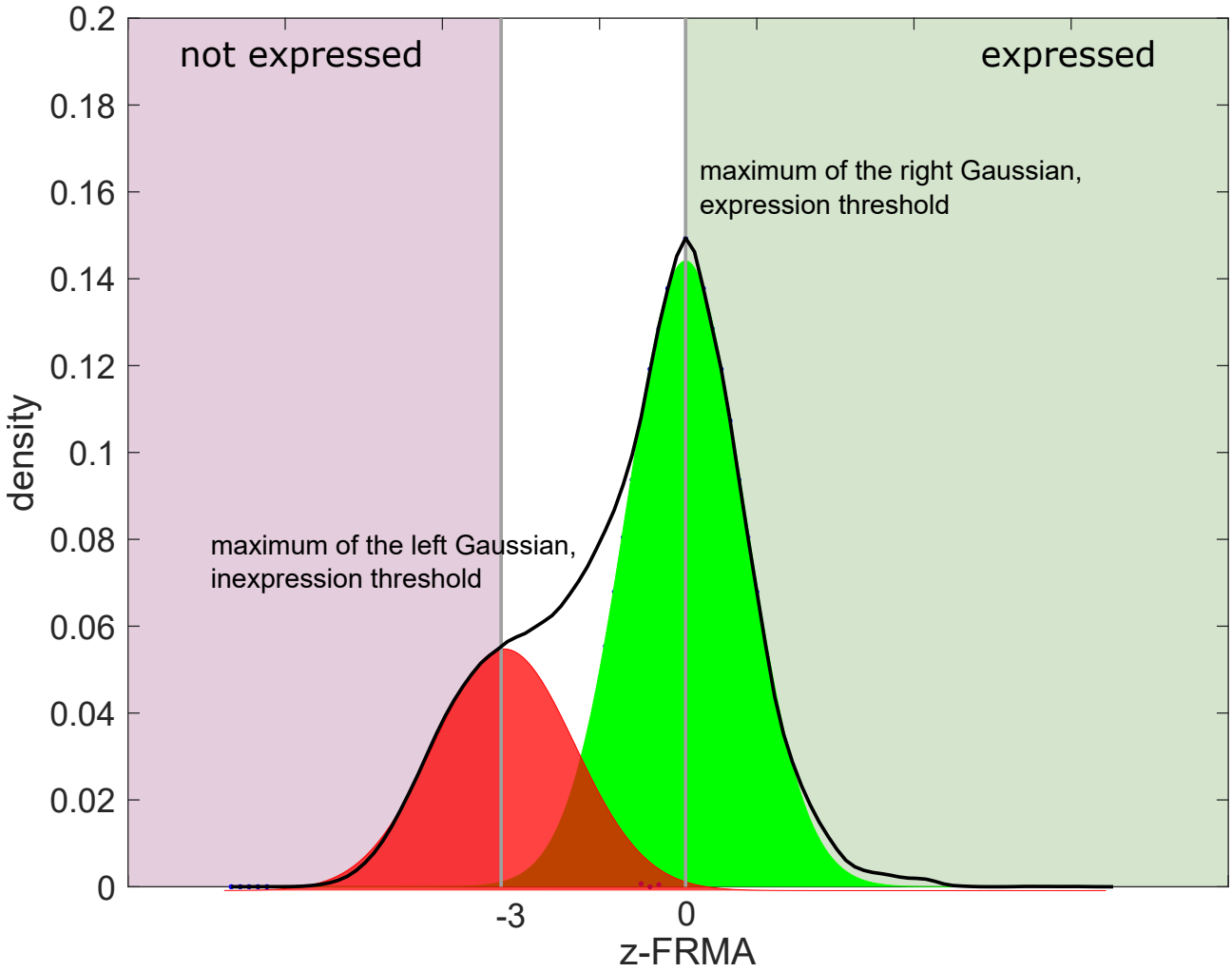

Figure S.1. Determination of the expression and inexpression threshold. The density plot of zFPKM converted log2-transformed FPKM is given by the black curve. The Gaussian curve in green corresponds to genes that are likely expressed. The red Gaussian curve corresponds to noise or leaky genes expression (uncontrolled expression), off-target read mapping or sequencing errors. In order to discretize the data, two thresholds are determined and applied: The expression threshold is the expression value corresponding to the maximum of the main signal peak (equal to a zFPKM score of 0) and the inexpression threshold is set at 3 standard deviations (3 z-scores) below the intensities values of the main peak. If the maximum of lowest peak has a zFPKM score $>$-3, then the latter is taken as inexpression threshold. If a gene has a zFPKM score below the value of the inexpression threshold (pink area), the gene is considered not expressed and a score of -1 (for not expressed) is assigned. If the zFPKM score of the considered gene is above 0 then a score of 1 (for expression) is assigned (green area). For all remaining genes a score of 0 (white area) is assigned.

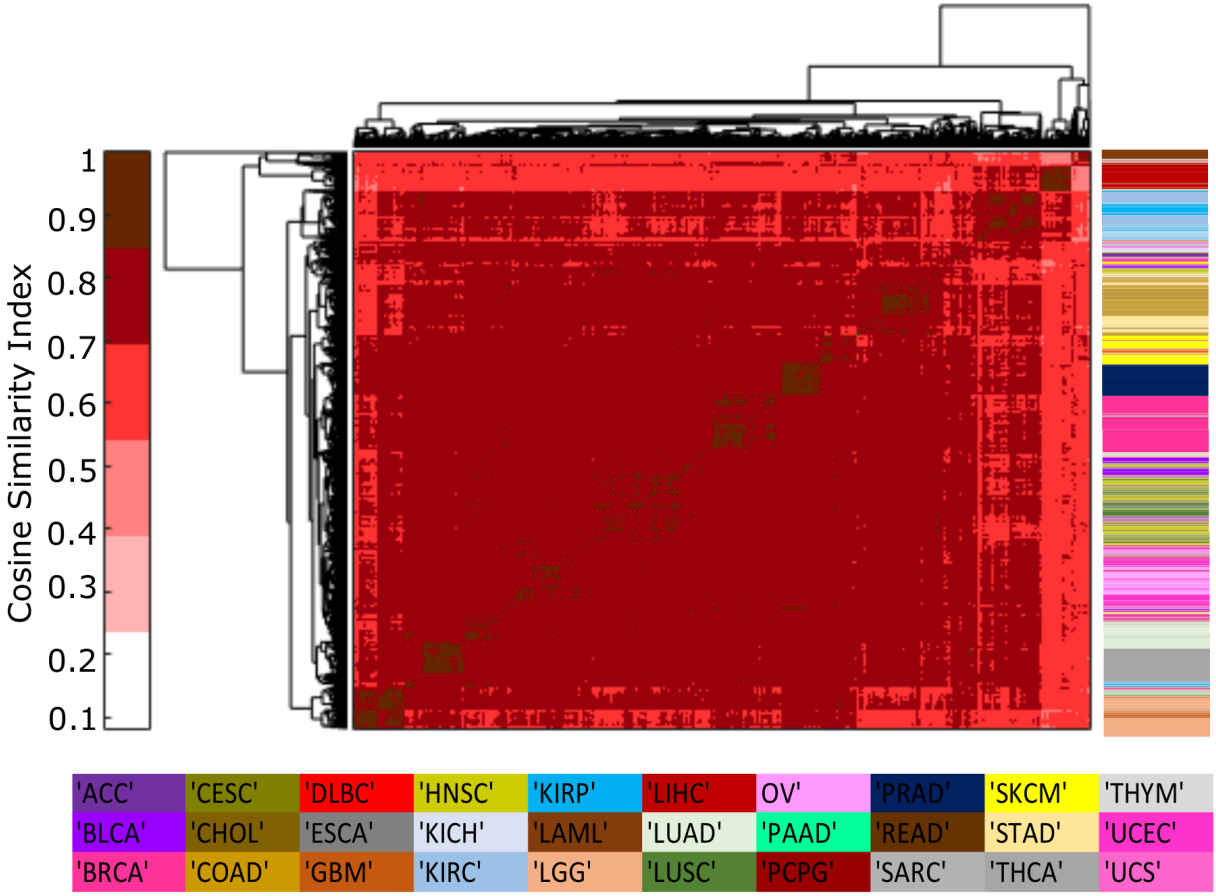

Figure S.2. The FASTCORMICS discretization step captures metabolic variations between different tissues. The discretized values (-1, 0, 1 for unexpressed, unknown, and expressed, respectively) of the metabolic genes of the 10,005 models from the TCGA dataset were clustered according to their cosine similarity index using the euclidean distance. Samples cluster according to their tissue of origin rather than in function of the healthy state of the sample. Overall, the samples show high similarity (cosine similarity index ¿ 0.5) with several sub clusters represented by a same tissue type. The clustergram displays 10,005 models of 30 different tissues: Adrenocortical carcinoma (ACC), Bladder Urothelial Carcinoma (BLCA), Breast invasive carcinoma (BRCA), Cervical squamous cell carcinoma and endocervical adenocarcinoma (CESC), Cholangiocarcinoma (CHOL), Colon adenocarcinoma (COAD), Lymphoid Neoplasm Diffuse Large B-cell Lymphoma (DLBL), Esophageal carcinoma (ESCA), Glioblastoma multiforme (GBM), Head and Neck squamous cell carcinoma (HNSC), (Kidney Chromophobe (KICH), Kidney Renal Papillary Cell Carcinoma (KIRP), Kidney Renal Clear Cell Carcinoma (KIRC), Acute Myeloid Leukemia (LAML), Brain Lower Grade Glioma (LGG) Liver hepatocellular carcinoma (LIHC), Lung adenocarcinoma (LUAD), Lung squamous cell carcinoma (LUSC), Ovarian serous cystadenocarcinoma (OV), Pancreatic adenocarcinoma (PAAD), Pheochromocytoma and Paraganglioma(PCPG), Prostate adenocarcinoma (PRAD), Rectum adenocarcinoma (READ), Sarcoma (SARC), Skin Cutaneous Melanoma (SKCM), Stomach adenocarcinoma (STAD), Thyroid carcinoma (THCA), Thymoma (THYM), Uterine Corpus Endometrial Carcinoma (UCEC), and Uterine Carcinosarcoma (UCS).

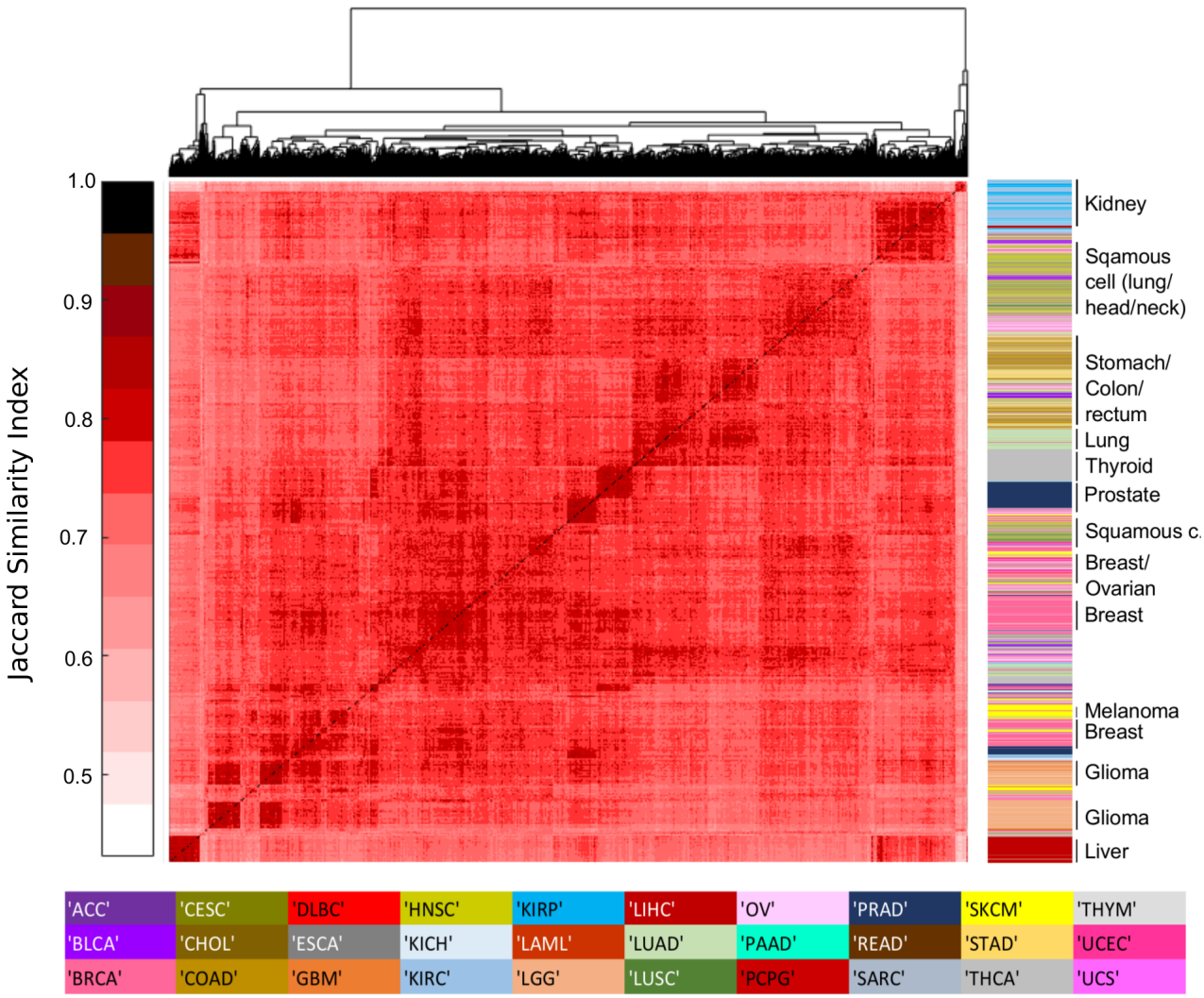

Figure S.3. FASTCORMICS captures metabolic alterations between tissues. Models from the same tissue of origin cluster together (high Jaccard similarity index), regardless if they were reconstructed from a cancer or a control sample. The tissue of origin has a higher impact on the model similarity then the healthy state.

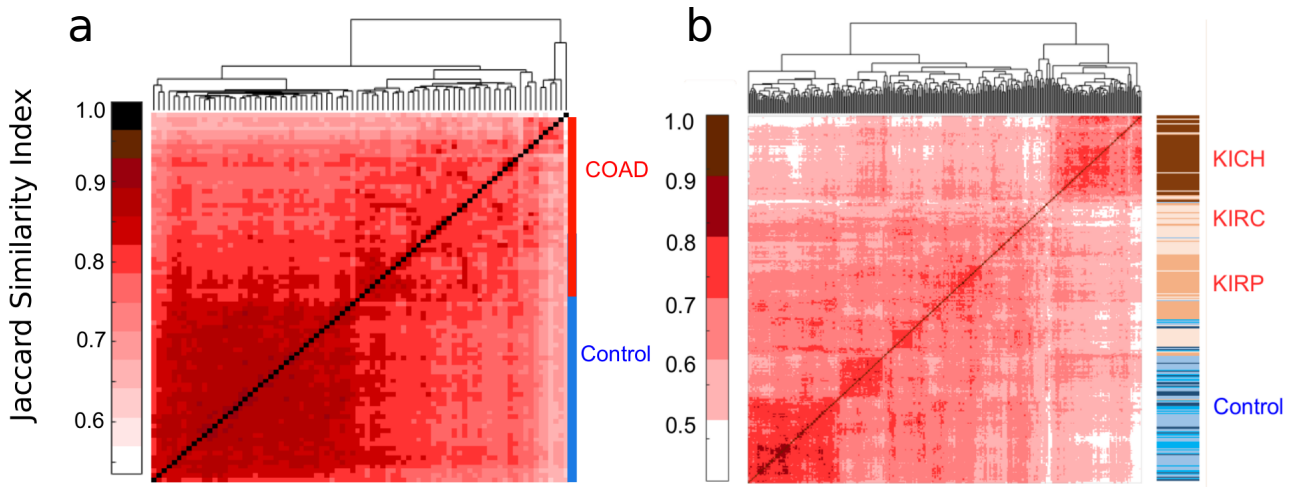

Figure S.4. rFASTCORMICS captures metabolic alterations between cancerous and healthy samples.
a) For individual tissues, such as colon, a clear segregation can be observed between the cancer and control models. The control models (blue) show higher inter-similarity compared to the cancer models, which are more heterogeneous.
b) For the kidney tissues, FASTCORMICS was able to capture metabolic variations between the controls and the three different cancer sub-types (Kidney Chromophobe (KICH), Kidney Renal Papillary Cell Carcinoma (KIRP) and Kidney Renal Clear Cell Carcinoma (KIRC)). The kidney models clustered in function of their subtypes and their label (control vs cancer).

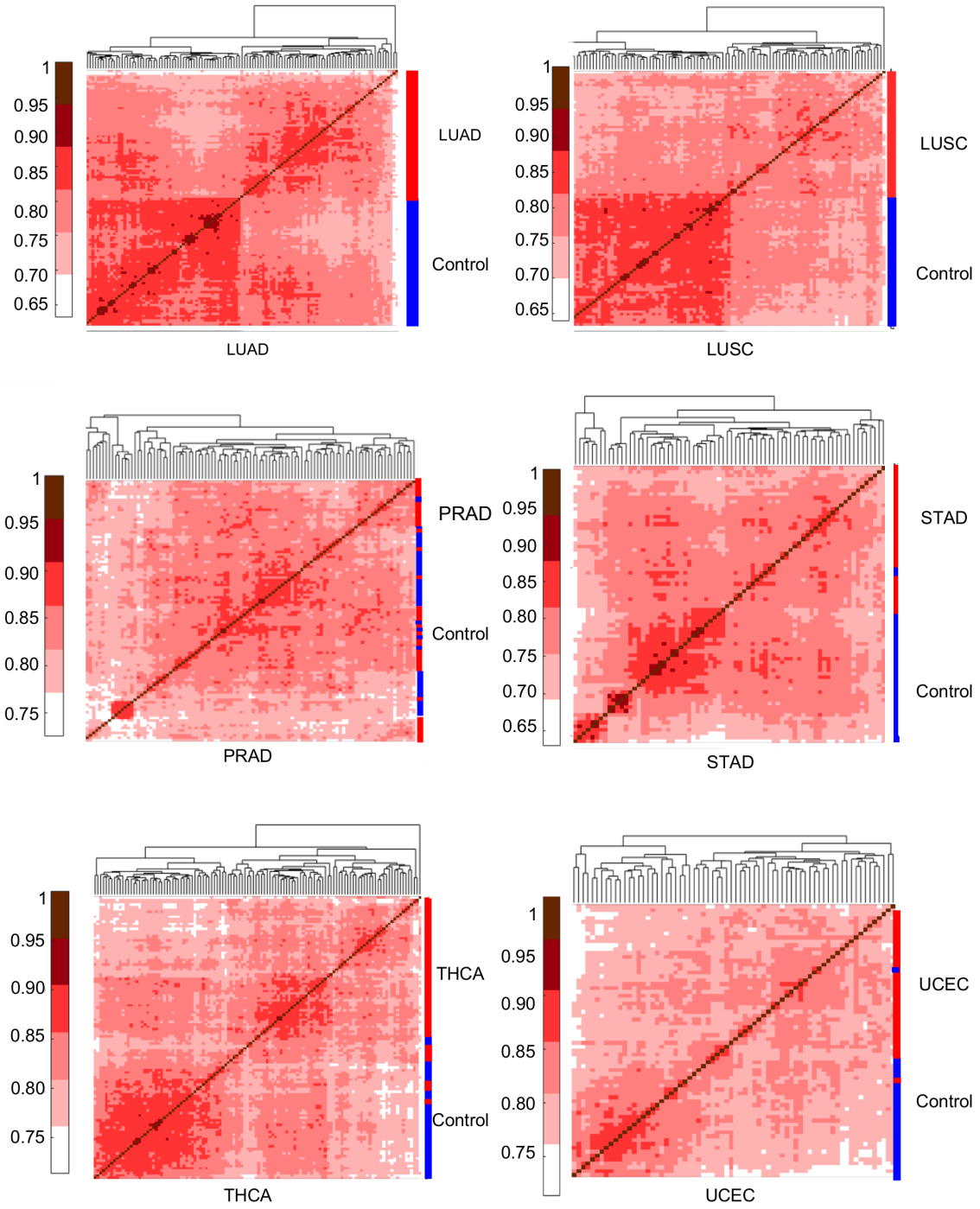

Figure S.5. The FASTCORMICS workflow captures metabolic variations between cancer and control samples. Cancer models (depicted by the red line next to the clustergram) showed high intra variability compared to the control models (blue line). However, a clear segregation could be observed between the cancer and control samples. The healthy models and the same number of cancer model from a same tissue were clustered in function of their Jaccard Similarity Index.

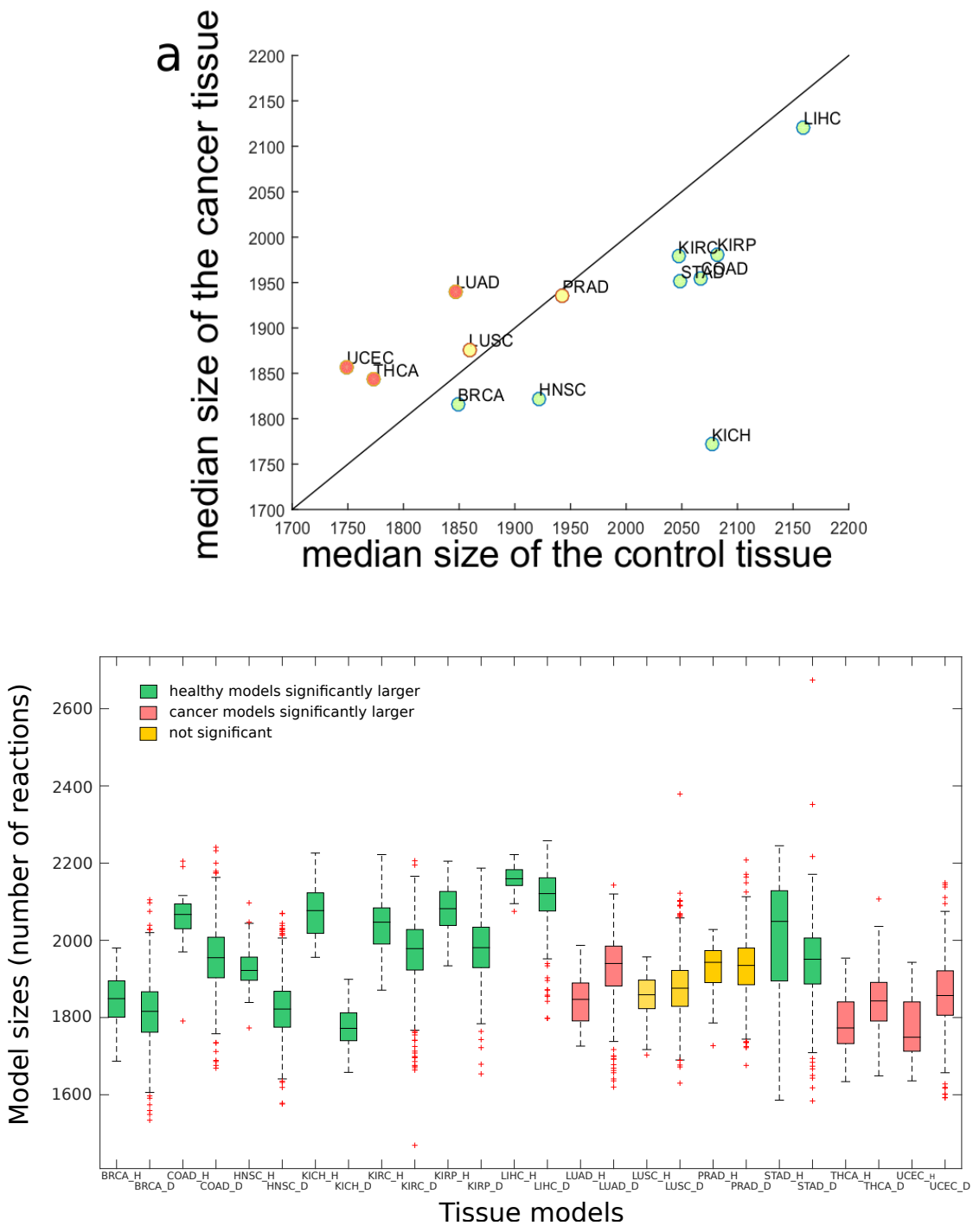

Figure S.6. Cancer models are overall smaller than their control models.
a) The median size of the cancer models is smaller for 9 tissues (green), greater for 3 (red), and not significantly different (yellow) for 2 tissues compared to the control models.
b) Boxplots showing the distribution in size for each cancer and control model from each of the 13 analysed tissues. The endings *_H* and *_D* in the tissue names represent healthy and cancer models, respectively. The green box plots illustrate tissues for which the cancer models are significantly smaller. The red box plots illustrate tissues for which the cancer models are significantly larger. The yellow box plots illustrate tissues for which no significant difference in model size can be observed between the cancer and control models.

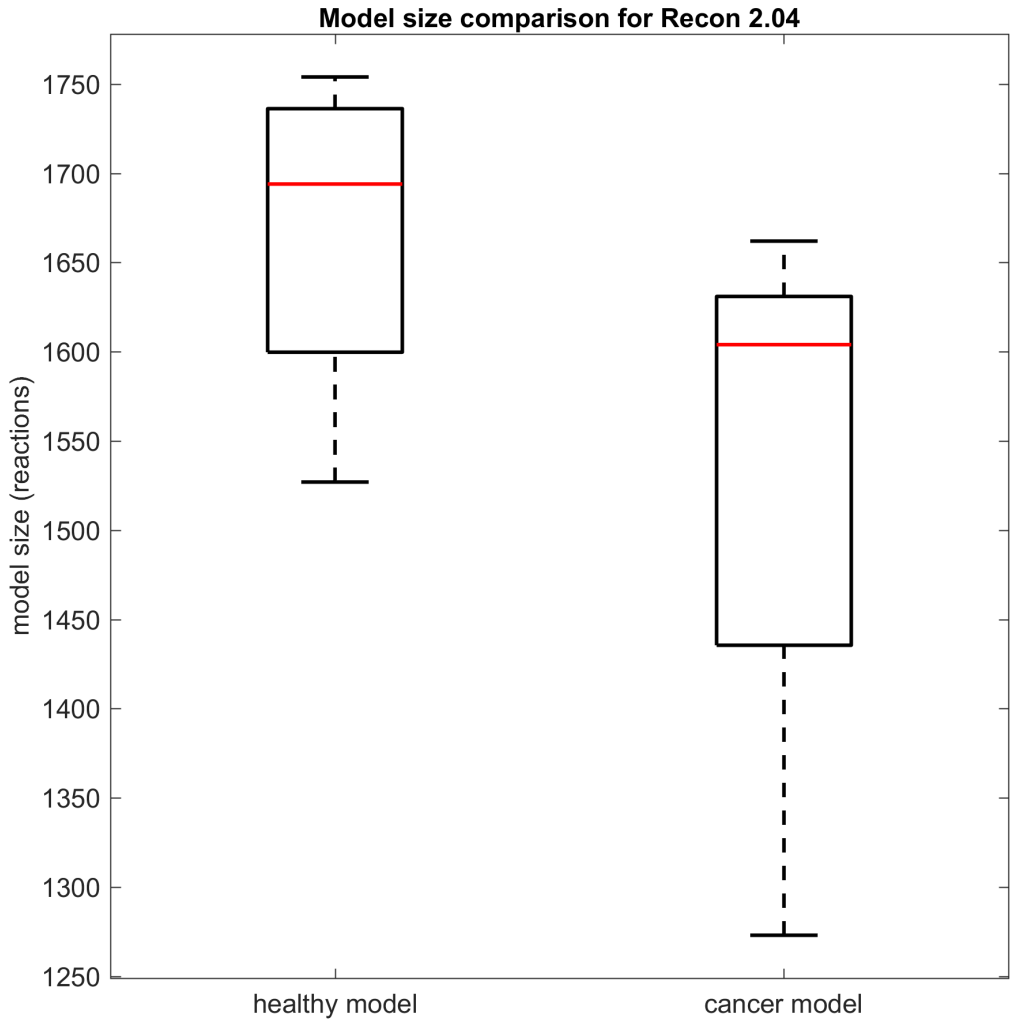

Figure S.7. The generic cancer models are smaller than the generic control models and have wider distribution. Generic models were built using Recon 2.04 as input. 13 models were used for the analysis, for both healthy and cancer state.

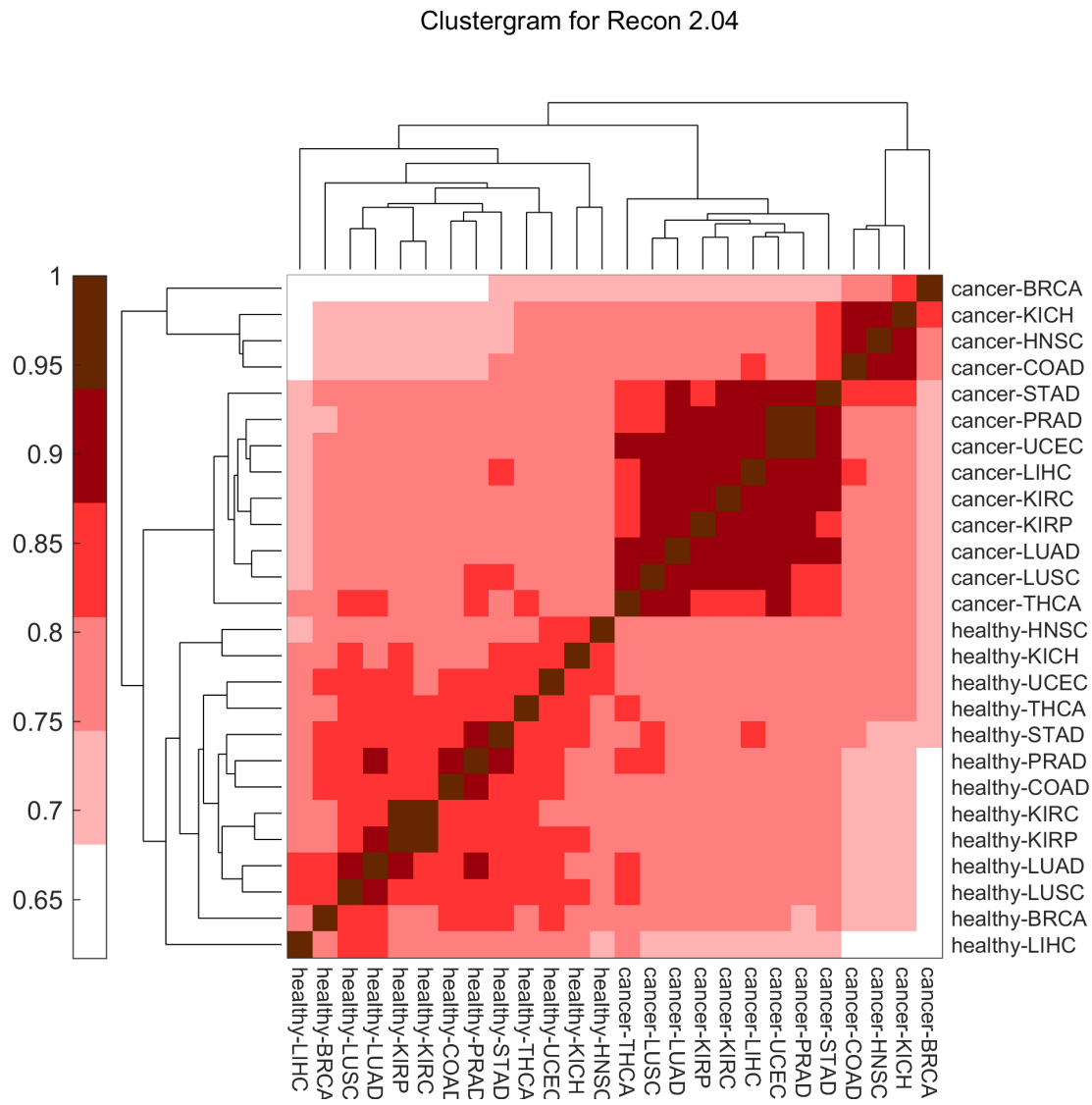

Figure S.8. FASTCORMICS is able to capture metabolic variations between the cancer and control models. The 13 generic cancer type models and the 13 corresponding generic control models cluster together whereas the cancer models are represented in two different clusters for both input models, accounting for the heterogeneity of cancer. The generic models were built with Recon 2.04 as input.

3.2 Machine learning: reaction and gene signatures

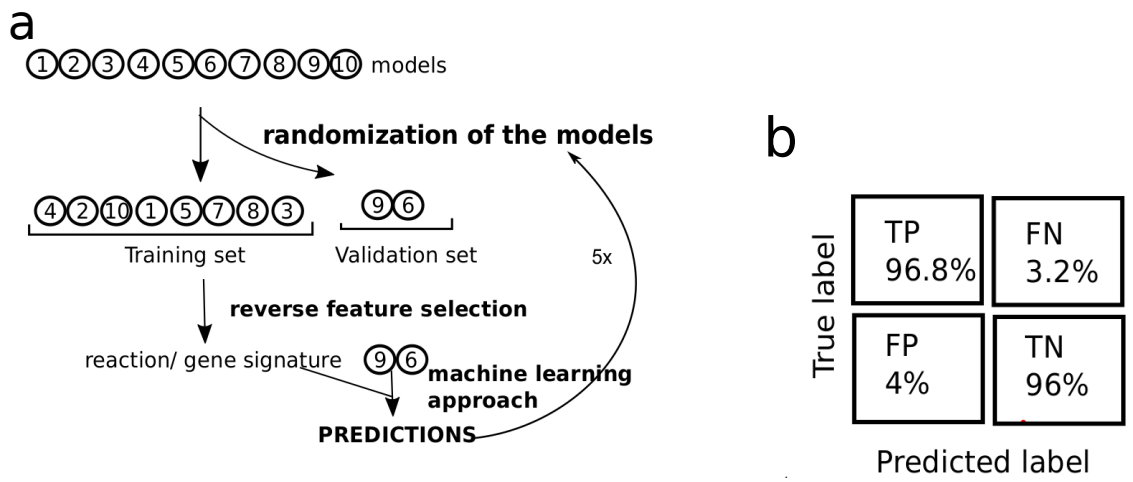

Figure S.9. Machine-learning approaches show that the metabolic alterations are not random but part of a rewiring strategy.
a) The models were randomized and split in a training set (80%) and a validation set (20%). A reverse feature selection approach was applied on the top most differentially active reactions/genes (features). At each round, one feature was removed and the machine learning models were trained on the training set to predict the labels of the validation set.
b) The confusion matrix for the hepatocarcinoma (LIHC) samples showed a high concordance between the predicted and the true labels. The TP (true positives), FN (false negatives), FP (false positives) and TN (true negatives) are respectively equal to 96.8%, 3.2%, 4% and 96%.

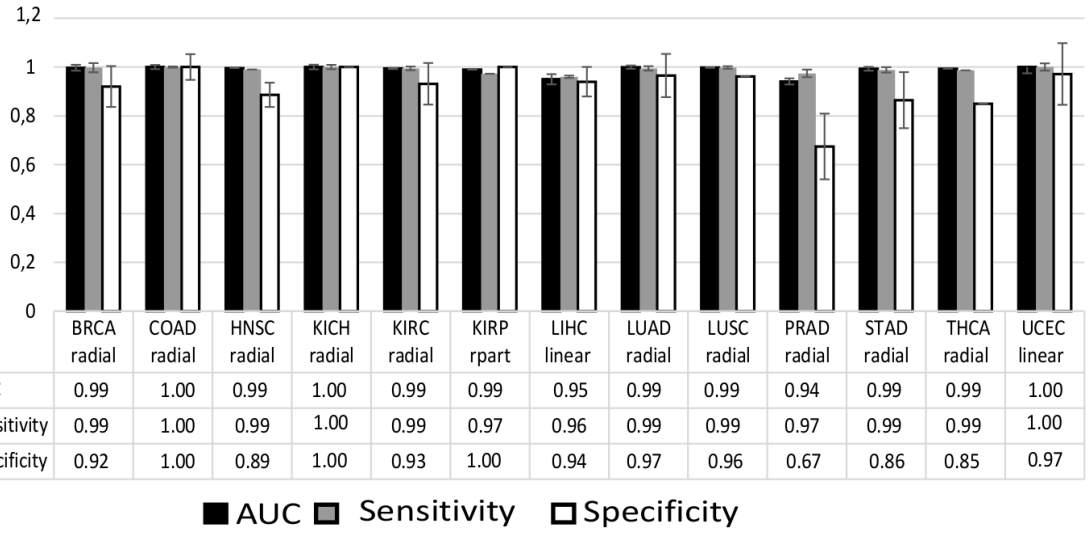

	BRCA radial	COAD radial	HNSC radial	KICH radial	KIRC radial	KIRP rpart	LIHC linear	LUAD radial	LUSC radial	PRAD radial	STAD radial	THCA radial	UCEC linear
AUC	0.99	1.00	0.99	1.00	0.99	0.99	0.95	0.99	0.99	0.94	0.99	0.99	1.00
Sensitivity	0.99	1.00	0.99	1.00	0.99	0.97	0.96	0.99	0.99	0.97	0.99	0.99	1.00
Specificity	0.92	1.00	0.89	1.00	0.93	1.00	0.94	0.97	0.96	0.67	0.86	0.85	0.97

Figure S.10. Reaction signatures: high accuracy, sensitivity and specificity for the 13 analysed tissues. The accuracy, sensitivity and specificity of the predictions, based on a 5-fold machine classifier using the reaction signatures for each tissue was above 0.94 for most tissues.

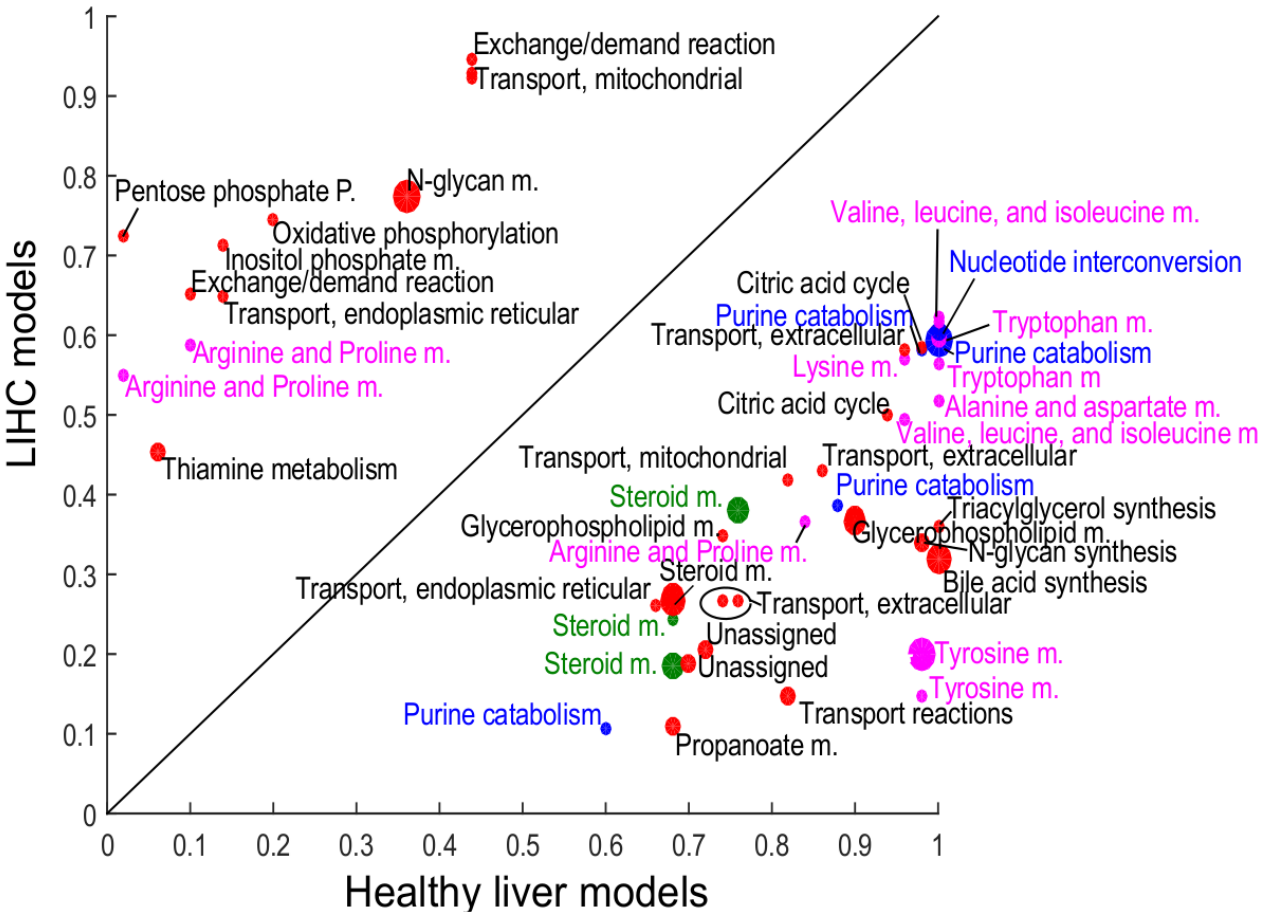

Figure S.11. Reaction signatures: LIHC shuts down pathways not required for survival or growth. Here only the top 100 reactions in the signature are plotted. Therefore, only the most differentially activated reactions (reactions that tend to be active in LIHC models and absent in controls or vice-versa) between LIHC and the liver control model was plotted against each other. Pathways that consume nucleotides (in blue), amino acids (pink), and cholesterol (green) are more often active in the control liver model and, overall, LIHC has fewer active reactions.

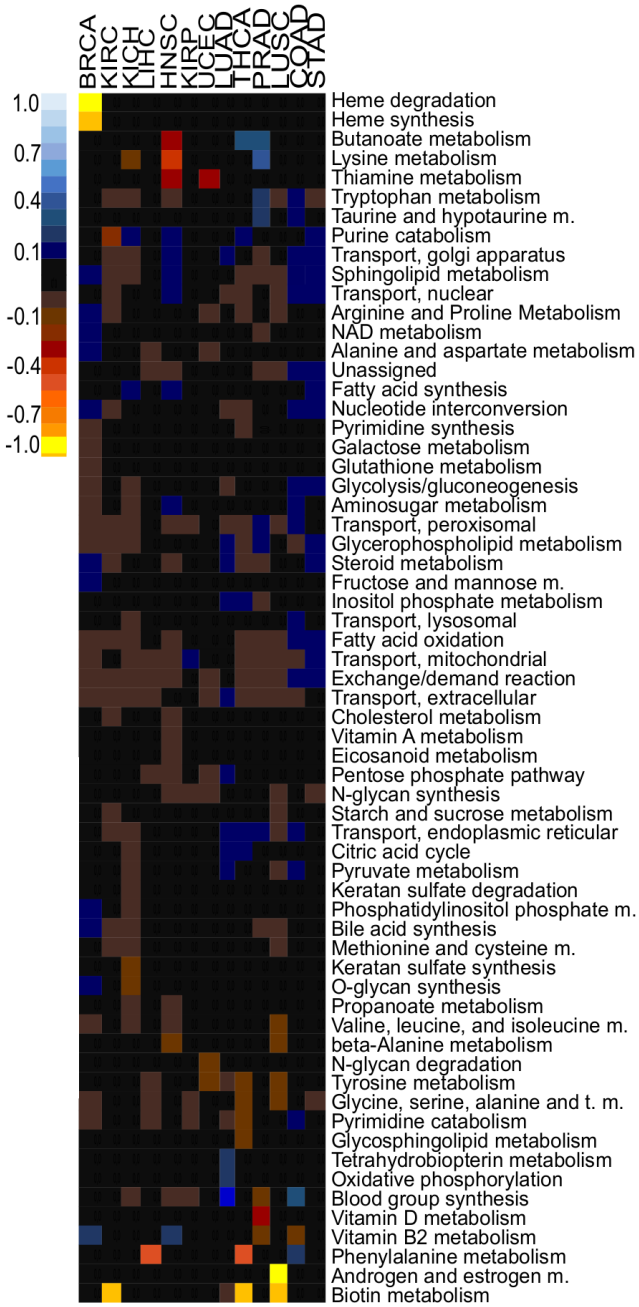

Figure S.12. Reaction signatures: Cancer cells shut down pathways not required for survival or growth. Reactions present in the reaction signatures tend to be more often active in control than in cancer models. The heatmap shows, for each pathway and tissue, the presence rate (fraction of reactions in a pathway which is present in the signatures) in the signatures. Higher presence rates in cancer and control are shown blue and orange shades, respectively.

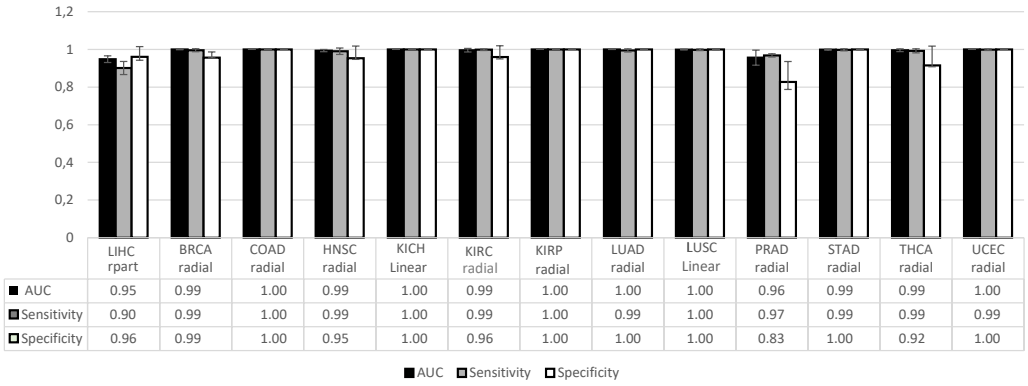

	LIHC rpart	BRCA radial	COAD radial	HNSC radial	KICH Linear	KIRC radial	KIRP radial	LUAD radial	LUSC Linear	PRAD radial	STAD radial	THCA radial	UCEC radial
AUC	0.95	0.99	1.00	0.99	1.00	0.99	1.00	1.00	1.00	0.96	0.99	0.99	1.00
Sensitivity	0.90	0.99	1.00	0.99	1.00	0.99	1.00	0.99	1.00	0.97	0.99	0.99	0.99
Specificity	0.96	0.99	1.00	0.95	1.00	0.96	1.00	1.00	1.00	0.83	1.00	0.92	1.00

Figure S.13. Gene signatures: high accuracy, sensitivity and specificity for the 13 analysed tissues. For all tissues, the gene signatures contained between 4 and 97 genes able to segregate between cancer and control models. 502 unique genes are found in total. The gene signatures were determined by a reverse feature selection approach and then used for cross-validation to asses the prediction power of the signatures. The accuracy of the prediction was higher than 94% for each tissue.

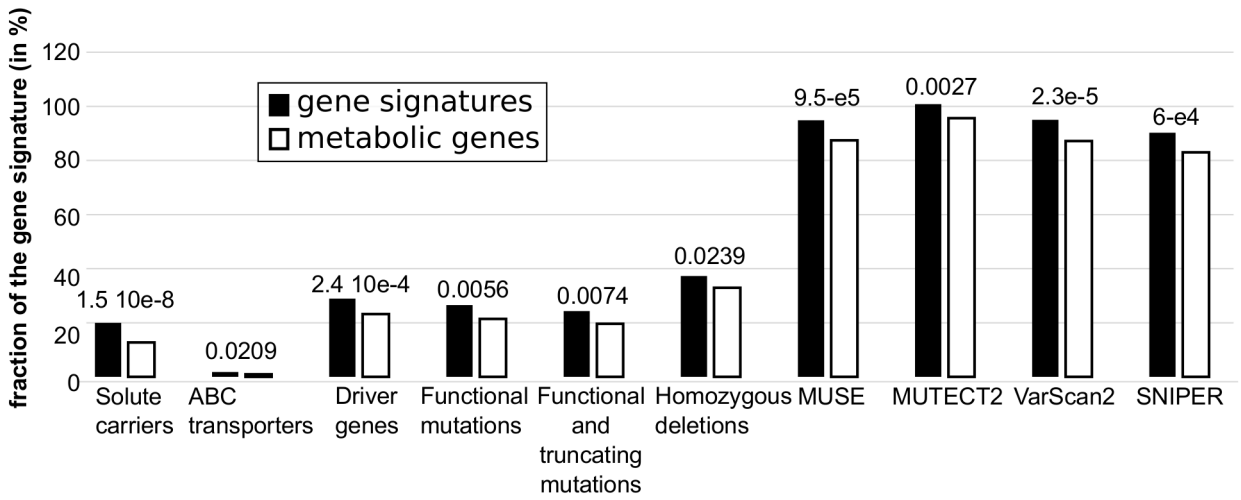

Figure S.14. Gene signatures are enriched for high-impact SNPs, loss-of-function mutations, transporters, and driver genes. The fraction of genes (from the 502 pooled gene signatures, in black), which code for transporters, driver genes, loss-of-function mutations, and genes predicted to have a high impact on the phenotype if mutated (determined by algorithms such as MUSE, MUTECT2, VarScan2 and sniper), is greater than in the metabolic genes (white).

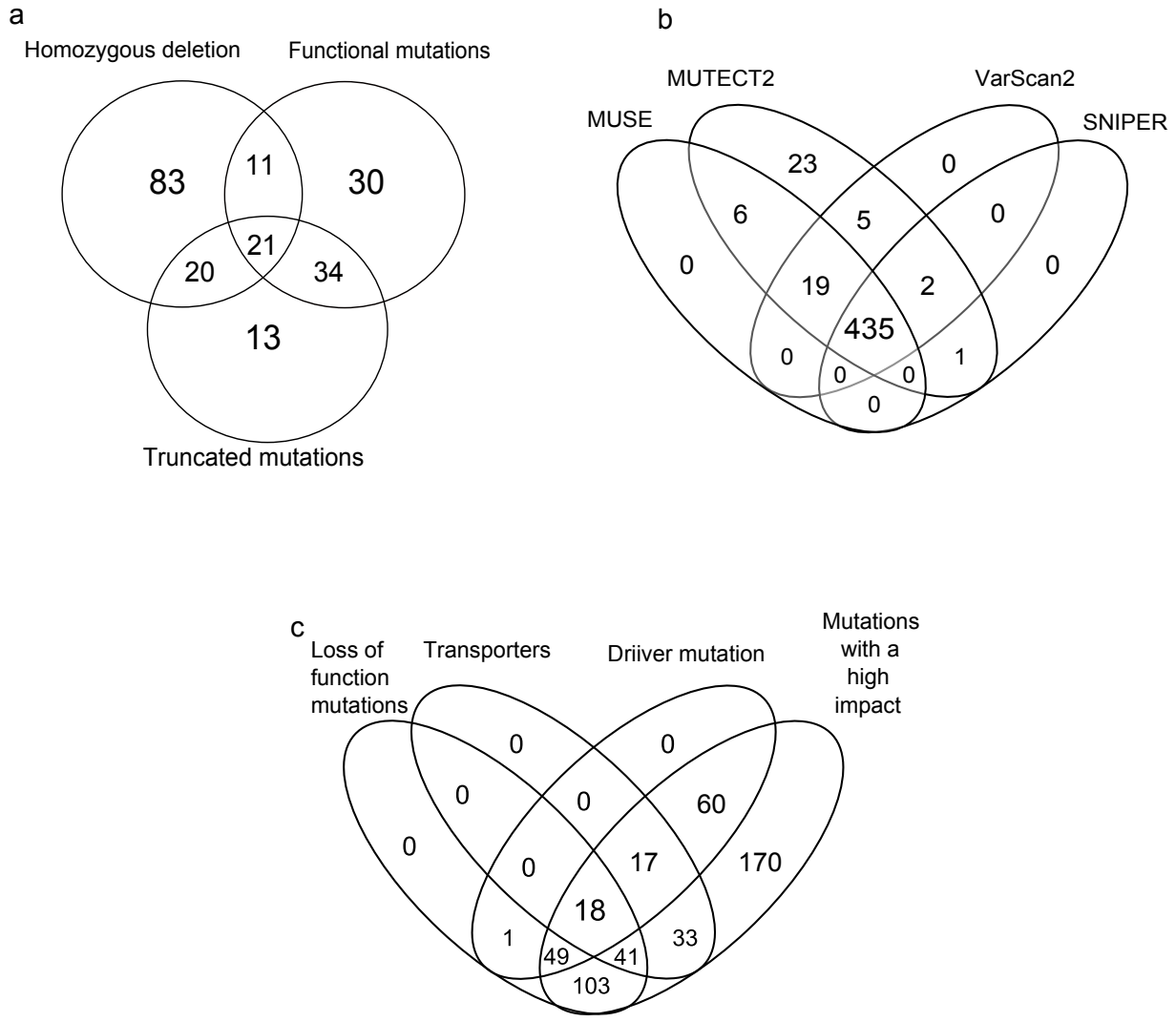

Figure S.15. Gene signatures carry mutations which have a high impact on the phenotype.
a) 212 genes in the signatures are homozygous deletions, functional, or truncated mutations (not mutually exclusive).
b) 435 genes have been found to highly affect the phenotype by all mutation calling algorithms (MUSE, MUTECT2, VarScan2 and sniper).
c) All genes but 1 from the signature were identified as mutations with a high impact where 211 were loss-of-function mutations, 109 were transporter and 144 driver mutations.

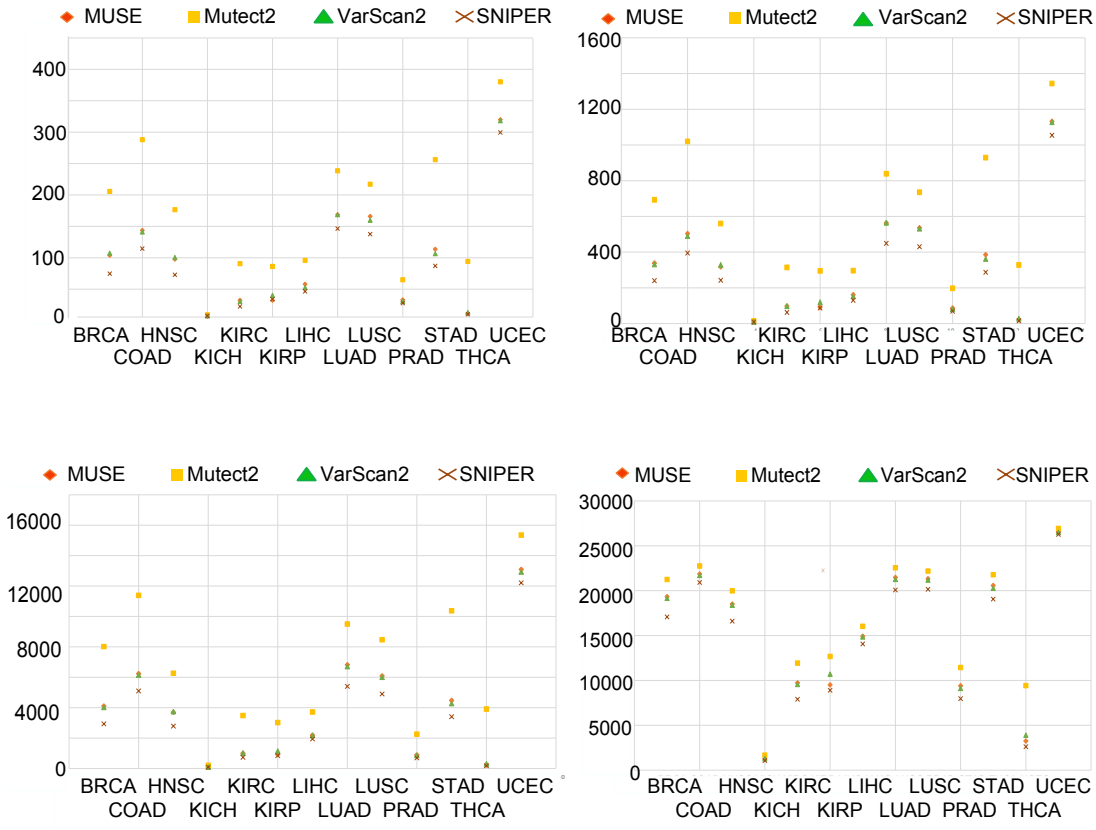

Figure S.16. Number of mutations detected by the mutation calling algorithm for different tissues. Pooled gene signatures (top left), metabolic genes (top right), genes that have a high impact (bottom left), and number of mutation with high, medium, and low impact on the phenotype (bottom right) detected in the different tissues by the mutation calling algorithms (MUSE, MUTECT2, VarScan2, and sniper).

3.3 The cancer core metabolism

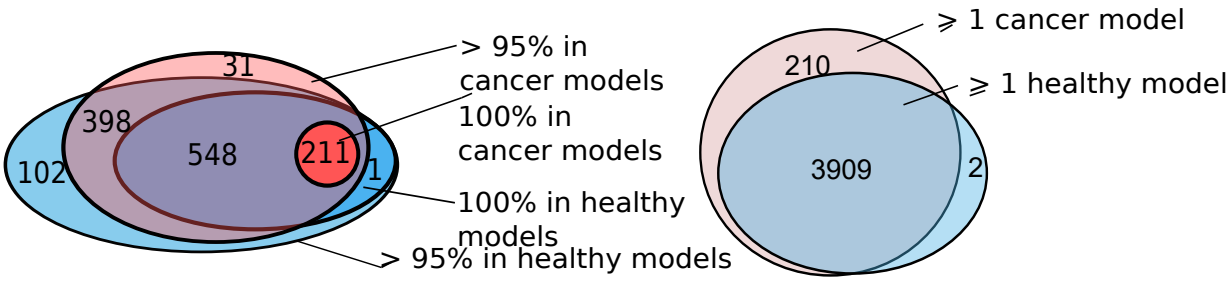

Figure S.17. Reactions: the cancer core metabolism is included in the control core metabolism.
All of the 10005 model were considered for this analysis. Left: 1,291 reactions were present in more than 95% of the models. 31 and 103 reactions were exclusive to cancer and control models, respectively. 211 reactions were always present in each cancer model, representing the cancer core metabolism. The control core metabolism comprised all reactions but one of the cancer core metabolism (total of 760 reactions) and was bigger than the cancer core metabolism.
Right: A total of 4,121 different reactions were present in at least one model. Only 2 reactions could not be found in the cancer models whereas 210 additional reactions were present in cancer.

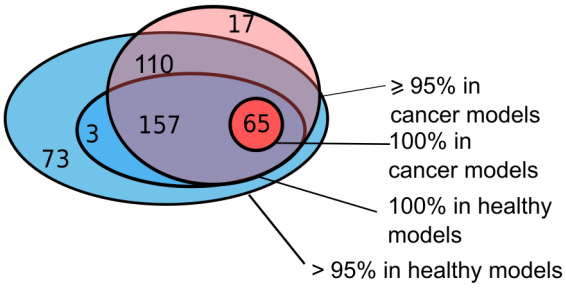

Figure S.18. Genes: the cancer core metabolism is included in the control core metabolism. The core metabolism of cancer cells (red), defined as the reactions present in 100% of the cancer metabolic models, is smaller than in the healthy core metabolism (blue). 17 genes are unique to the cancer models while 76 genes are unique to the control models. All of the 10005 model were considered for this analysis.

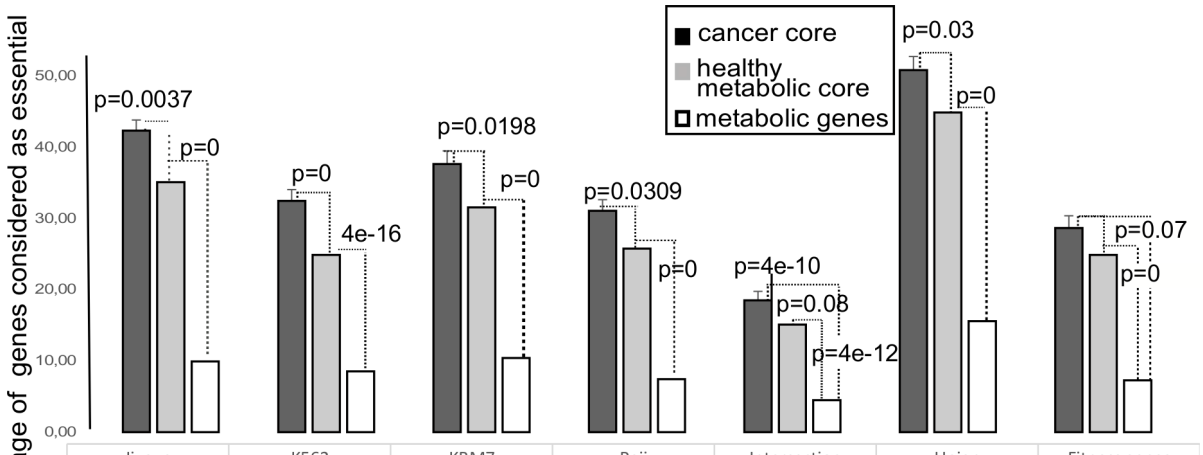

Jiyoye	K562	KBM7	Raji	Intersection	Union	Fitness genes
42.34	32.49	37.64	31.09	18.50	50.58	28.68
35.11	24.89	31.56	25.78	15.11	44.89	24.89
9.94	8.55	10.41	7.44	4.48	15.58	7.27

Figure S.19. Genes: the cancer core metabolism is enriched for essential genes. The cancer core metabolic genes (black) and the healthy core metabolic genes (grey) were significantly enriched for essential genes compared to the metabolic genes (white). A list was retrieved from[21] who identified essential genes by CRISPR-Cas9 screens in the Jiyoye, K562, KBM7, and Raji cancer cell lines. The intersection represents genes which were found to be essential in each of the 4 cell lines and the union in any of the 4 cell lines. A list of fitness genes (essential in 3 out of 5 TKO cell lines) was retrieved from.[22]

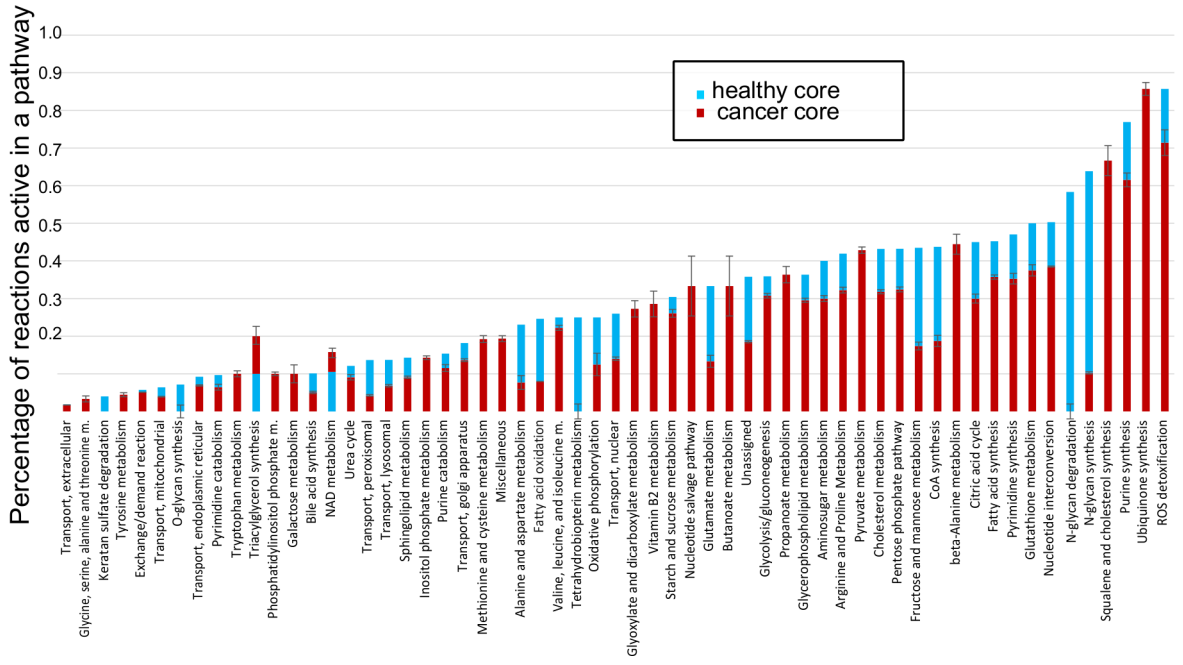

Figure S.20. The cancer core metabolism has lower pathway activity. Branches of metabolic pathways are shut down in the cancer models (red) when compared to their healthy counterparts (blue), resulting in a smaller percentage of active reactions per pathway. For example, the presence rate of the ROS detoxification pathway for cancer and healthy are 71% and 86%, respectively.

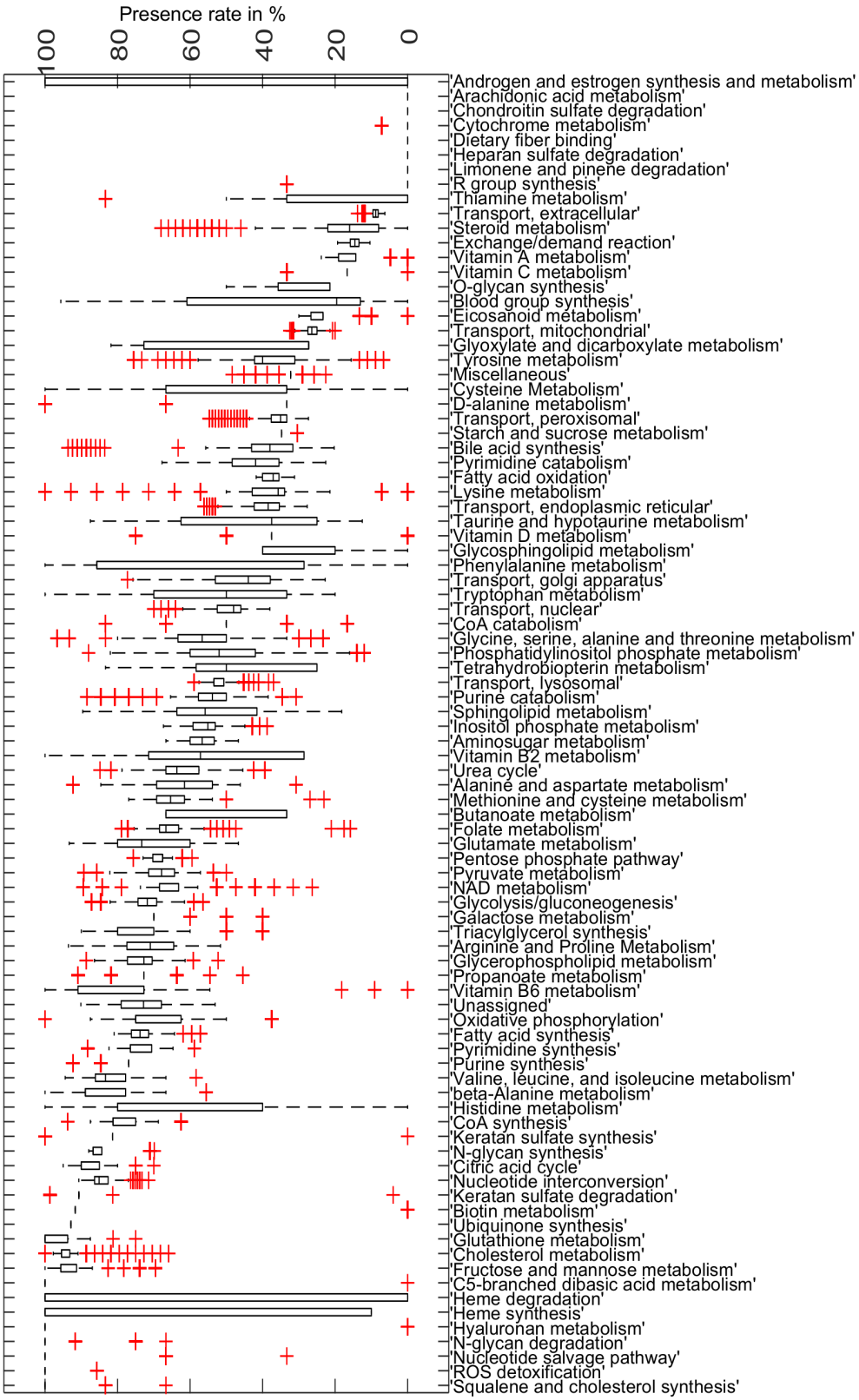

Figure S.21. Control models: reaction presence rates across 90 pathways. Distribution of the active reactions for each pathway present in Recon 2.04. 741 healthy models were used.

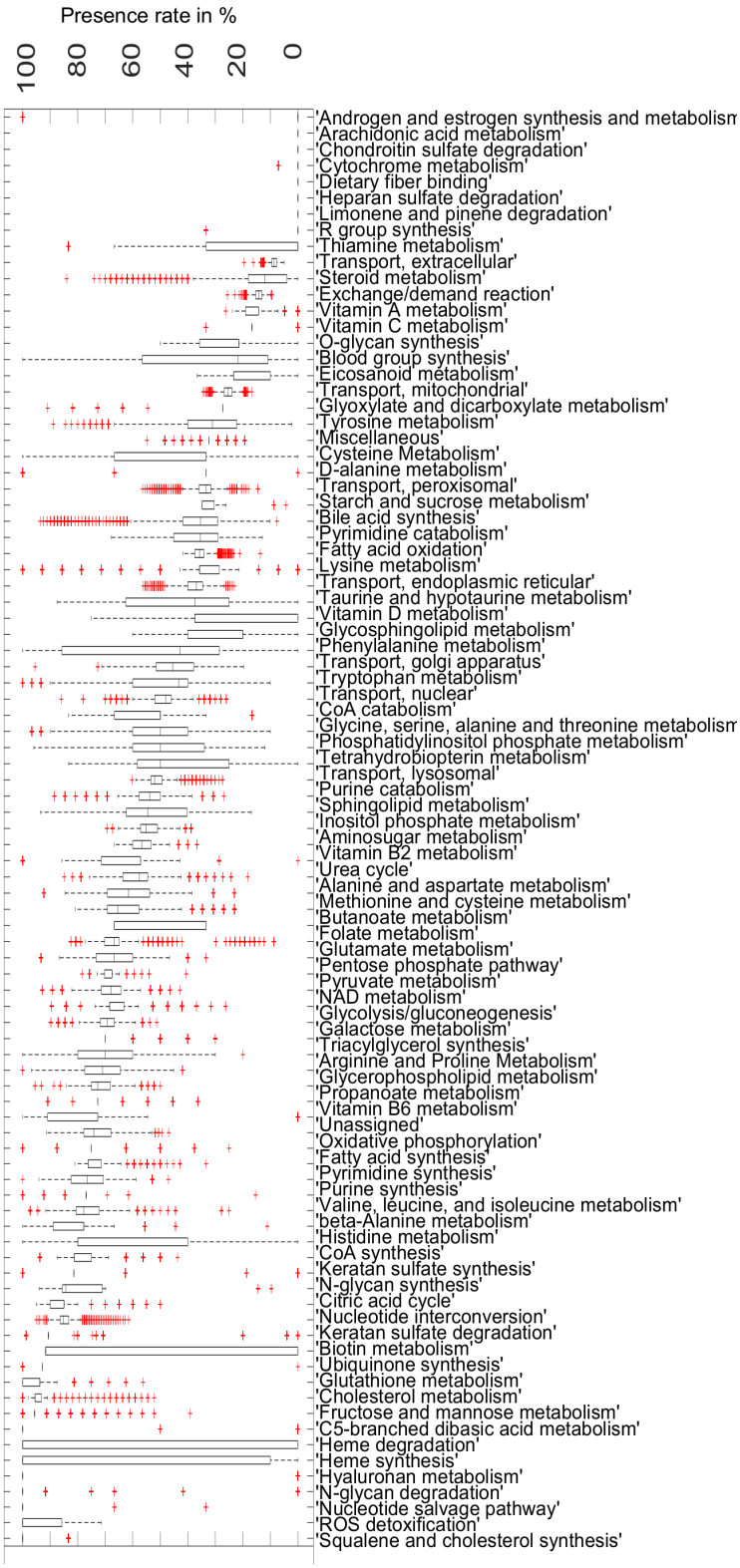

Figure S.22. Cancer models: reaction presence rates across 90 pathways. Distribution of the active reactions for each pathway present in Recon 2.04. 9,264 cancer models were used.

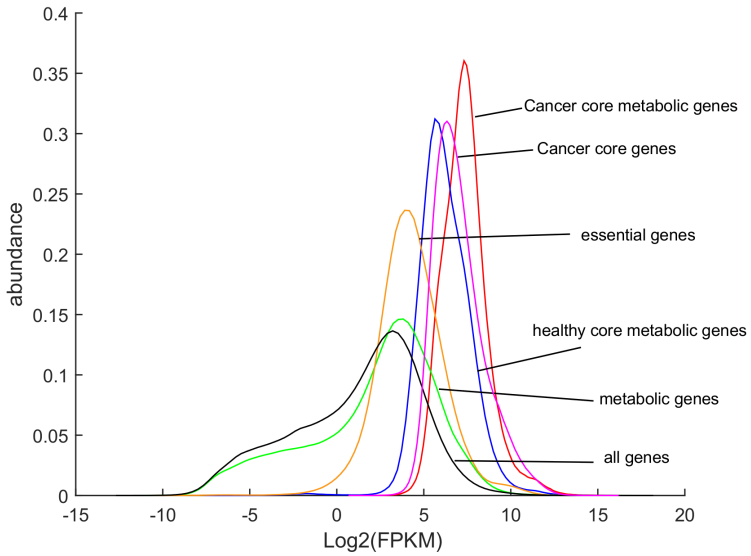

Figure S.23. The cancer core metabolic genes have higher expression values and abundance. Abundance of the log2(FPKM) expression values for the different genes: cancer core genes (pink), cancer core metabolic genes (red), essential genes (yellow), healthy core metabolic genes (blue), metabolic genes (green), and all genes (black).

3.4 In silico gene deletions and drug repurposing

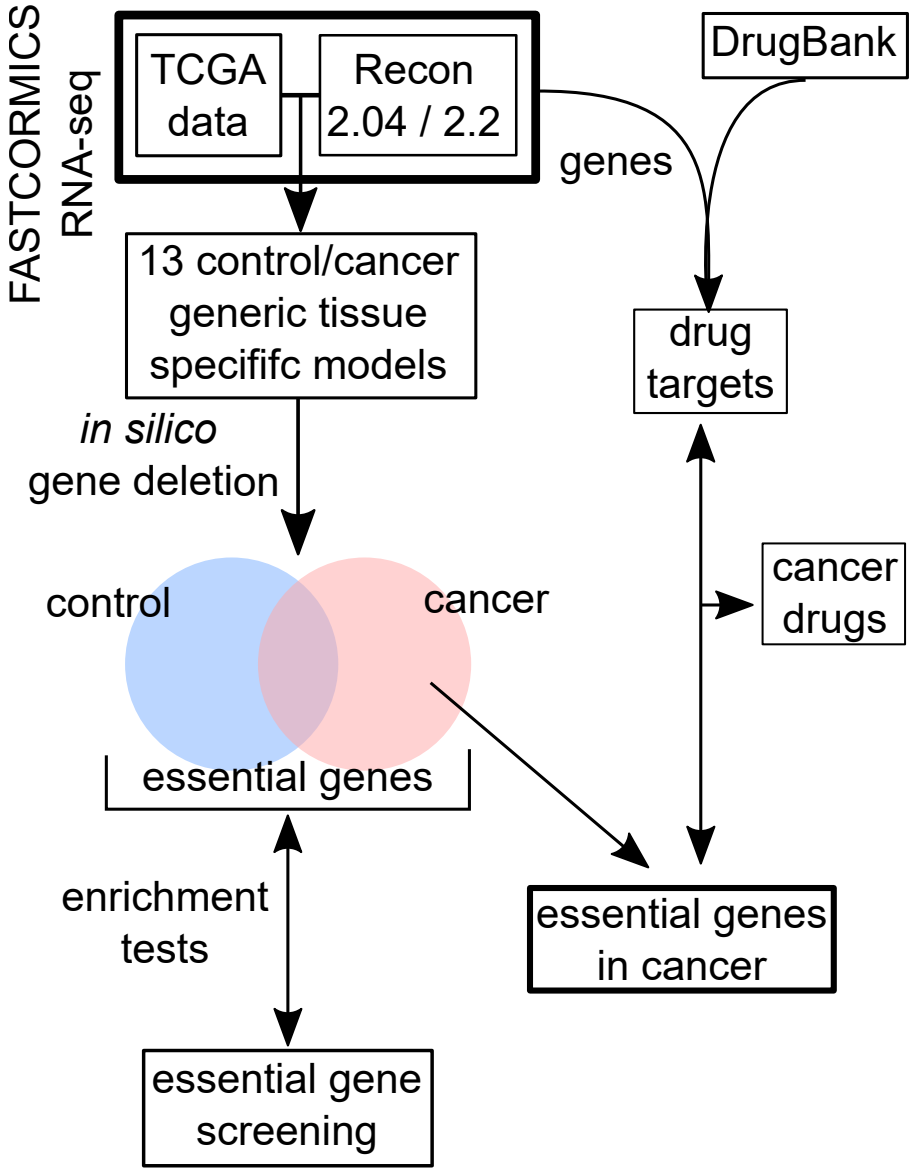

Figure S.24. Drug repurposing workflow based on rFASTCORMICS. 13 cancer and control generic tissue-specific models were reconstructed using the TCGA and Recon X as input for rFASTCORMICS. Essential genes for each tissue were determined using *in silico* gene deletions while optimizing for the ATP demand or biomass reaction as objective function. The predicted essential genes were tested for enrichments in known essential gene screenings.[21–23] The DrugBank was used to retrieve drug targets using for the genes present in the models. The drug targets were then compared to the predicted essential genes in cancer and, in a last step, cancer drugs are retrieved.

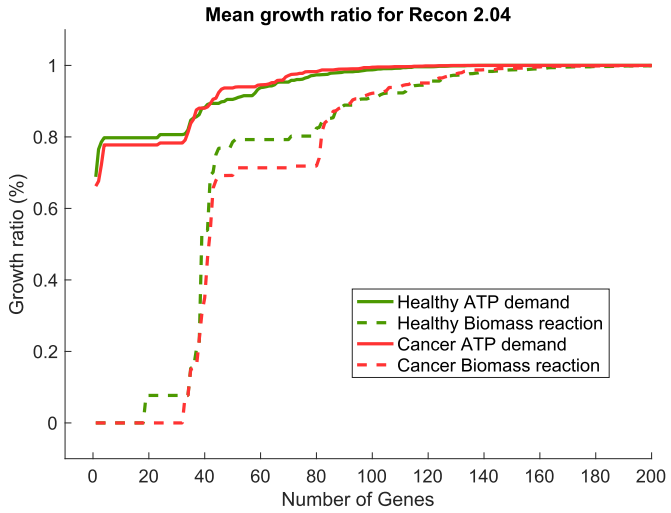

Figure S.25. Mean growth ratios for ATP and biomass. The ATP demand is more robust to gene deletions than the biomass production. Control and cancer models are affected differently by *in silico* gene deletions, here represented as mean ratios from all 13 generic models. The ATP demand is never completely shut down, the lowest mean ratio being 0.6883 (cancer) and 0.6498 (healthy). On the other hand, gene deletions affect the biomass production differently, producing intermediate phenotypes. Deletion of 33 and 18 genes results in a growth ratio of 0 in cancer and healthy, respectively.

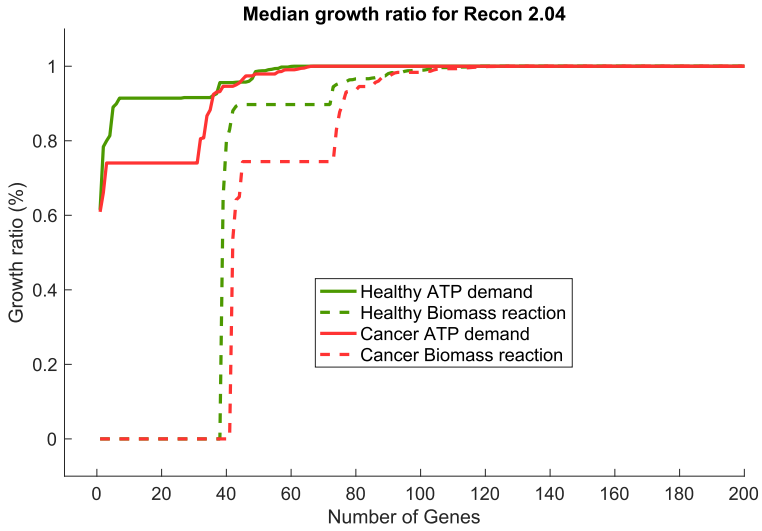

Figure S.26. Median growth ratios for ATP and biomass. The ATP demand is more robust to gene deletions than the biomass production. Control and cancer models are affected differently by *in silico* gene deletions, here represented as median ratios from all 13 generic models. The ATP demand is never completely shut down, the lowest ratio can be observed around 0.7. On the other hand, gene deletion affect the biomass production differently producing intermediate phenotypes.

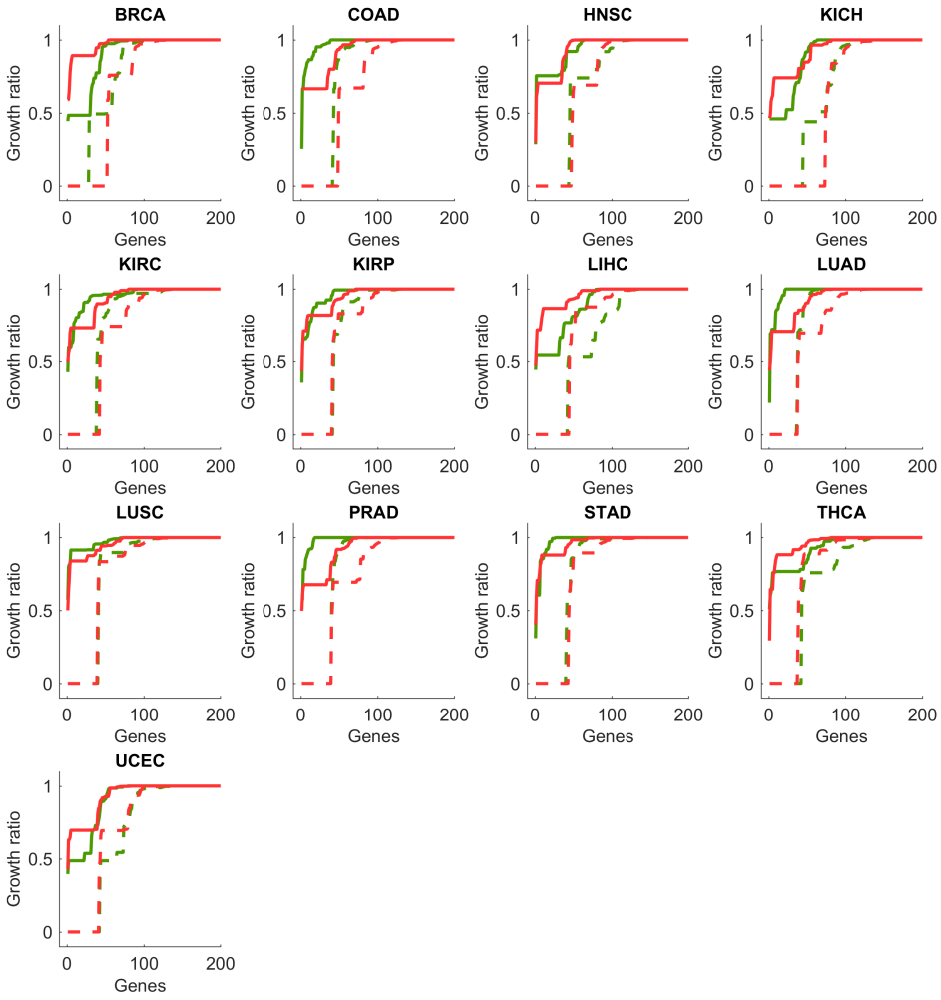

Figure S.27. Growth ratios for ATP and biomass for all tissues reconstructed from Recon 2.04. In general, single gene deletion has an higher impact on the biomass production than on ATP demand, regardless of the tissue.

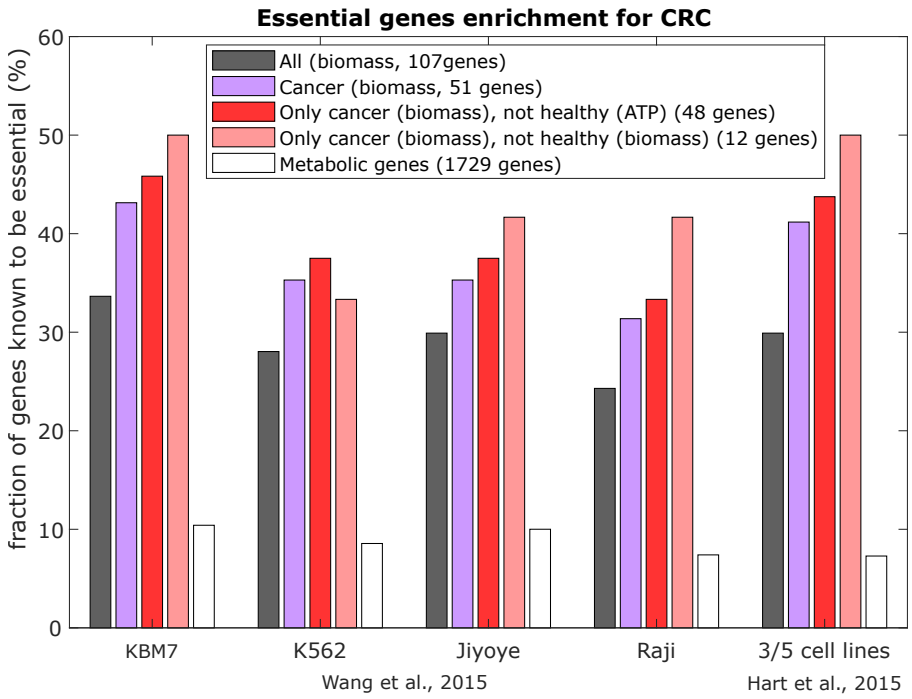

Figure S.28. Predicted essential genes in CRC are enriched for known essential genes. The predicted essential genes were compared to five different essential gene screenings from.[21,24] High enrichments are found in the cancer-specific essential genes if compared to the metabolic genes. See Table S.5 for a more detailed explanation of the figure legend.

3.5 Validation

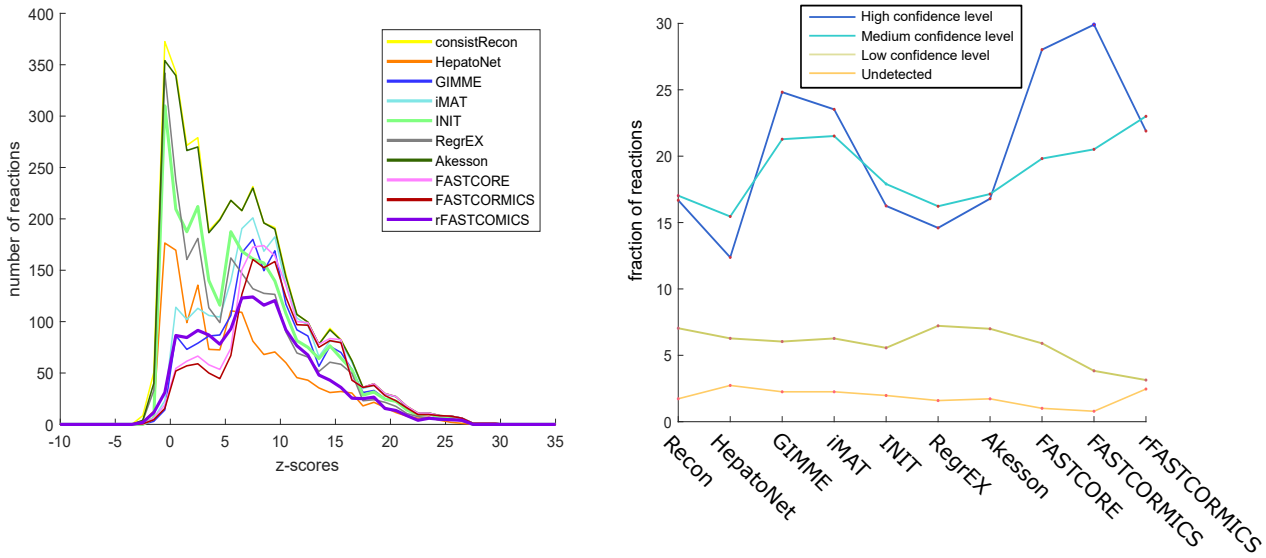

Figure S.29. Models reconstructed with rFASTCORMICS are enriched for reactions with a high confidence level. Unlike the other models, rFASTCORMICS was run with RNA-seq data as input. Models reconstructed with FASTCORMICS show high confidence scores at the transcriptomic level and behave similarly to the models reconstructed with FASTCORE (left). Models reconstructed with FASTCORMICS show an enrichment for of reactions associated to high and medium confidence levels at the proteome level (human Protein atlas) (right).

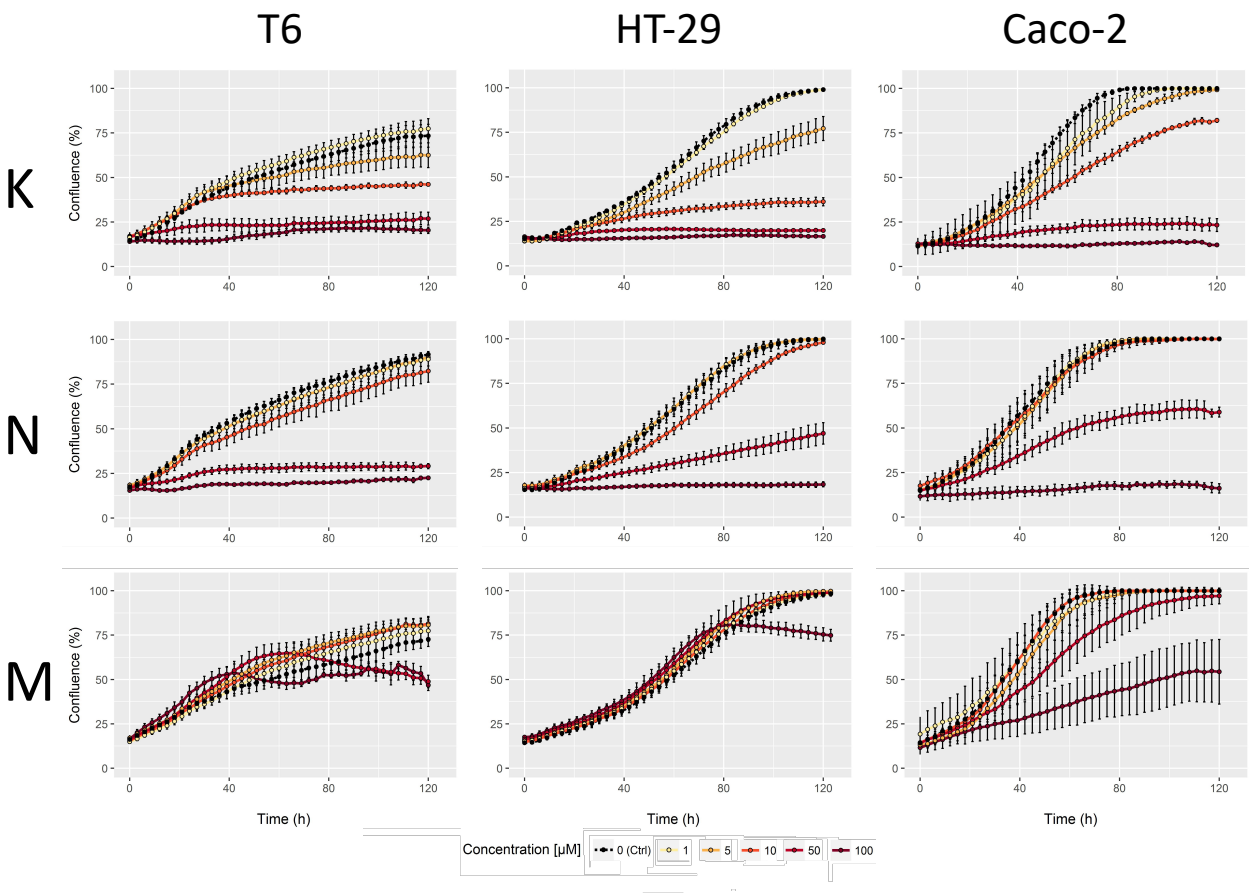

Figure S.30. Effect of candidate drugs on primary and commercial colorectal cancer cells. 12,000 T6 cells, HT29 cells, or Caco-2 cells were seeded in 100 μL of growth medium into each well of a 96 well plate. 24 hours afer seeding ,medium in each well was exchanged and cells were treated with the corresponding drugs Ketoconazole (K), Naftifine (N), and Mimosine (M),at different concentraer seeding, medium in each well was exchanged and cells were treated with the corresponding drugs Ketoconazole (K), Naftifine (N), and Mimosine (M), at different concentraer seeding, medium in each well was exchanged and cells were treated with the corresponding drugs Ketoconazole (K), Naftifine (N), and Mimosine (M), at different concentrations. Cellular confluence was measured every 3 hours over 5 days. Data show representative experiments of threebiological replicates per cell line. Data points represent mean confluence $\pm$ SD of 6 wells.

4. Supplementary Tables

Table S.1. Cancer abbreviations and full names. Explanation of the abbreviations used in the TCGA dataset.

Cancer abbreviation	Full name of cancer
ACC	Adrenocortical carcinoma
BLCA	Bladder urothelial carcinoma
BRCA	Breast invasive carcinoma
CESC	Cervical squamous cell carcinoma and endocervical adenocarcinoma
CHOL	Cholangiocarcinoma
COAD	Colon adenocarcinoma
DLBC	Lymphoid neoplasm diffuse large B-cell lymphoma
ESCA	Esophageal carcinoma
GBM	Glioblastoma multiforme
HNSC	Head and neck squamous cell carcinoma
KICH	Kidney chromophobe
KIRC	Kidney renal clear cell carcinoma
KIRP	Kidney renal papillary cell carcinoma
LAML	Acute myeloid leukemia
LGG	Brain lower grade glioma
LIHC	Liver hepatocellular carcinoma
LUAD	Lung adenocarcinoma
LUSC	Lung squamous cell carcinoma
OV	Ovarian serous cystadenocarcinoma
PAAD	Pancreatic adenocarcinoma
PCPG	Pheochromocytoma and paraganglioma
PRAD	Prostate adenocarcinoma
READ	Rectum adenocarcinoma
SARC	Sarcoma
SKCM	Skin cutaneous melanoma
STAD	Stomach adenocarcinoma
THCA	Thyroid carcinoma
THYM	Thymoma
UCEC	Uterine corpus endometrial carcinoma
UCS	Uterine carcinosarcoma

Table S.2. Model size overview for each tissue. The number of control and cancerous samples as well as the median sizes of the models is given for each tissue type. NaN was assigned to the median size of healthy control and cancer models for tissues for which no samples were available.

Cancer abbreviation	Number of healthy models	Number of cancer models	Median size of healthy models	Median size of cancer models
ACC	0	79	NaN	1882
BLCA	19	414	1897	1898
BRCA	113	1119	1849	1816
CESC	3	306	1689	1835
CHOL	9	0	2164	NaN
COAD	41	483	2067	1955
DLBC	0	48	NaN	1811
ESCA	13	0	1928	NaN
GBM	5	170	1826	1818
HNSC	44	504	1922	1822
KICH	25	66	2077	1772
KIRC	72	542	2047	1978
KIRP	32	291	2082	1981
LAML	0	178	NaN	1465
LGG	0	532	NaN	1743
LIHC	50	374	2159	2121
LUAD	59	541	1847	1940
LUSC	51	502	1859	1876
OV	0	430	NaN	1875
PAAD	4	0	1909	NaN
PCPG	3	0	1906	NaN
PRAD	52	502	1943	1935
READ	10	167	2045	1967
SARC	2	0	1985	NaN
SKCM	1	472	1889	1748
STAD	37	420	2049	1951
THCA	59	513	1773	1843
THYM	2	0	1722	NaN
UCEC	35	554	1749	1857
UCS	0	57	NaN	1813

Table S.3. Optional medium composition used to reconstruct the context-specific models. The medium composition is used to constrain the uptakes or exchange reactions during the model building process. The metabolite column represents the metabolites as found in the model.mets field in Recon 2.04.

metabolite	metabolite Name
4hpro_LT[e]	trans-4-hydroxy-L-proline
5adtststerone[e]	17beta-hydroxy-5alpha-androstan-3-one
5mta[e]	5-Methylthioadenosine
Lcystin[e]	L-cystine
ala_L[e]	L-alanine
arg_L[e]	L-argininium(1+)
asn_L[e]	L-asparagine
asp_L[e]	L-aspartate(1-)
bilirub[e]	bilirubin(2-)
btn[e]	Biotin
ca2[e]	calcium(2+)
chol[e]	Choline
cl[e]	Chloride
co2[e]	carbon dioxide
cys_L[e]	L-cysteine
fe2[e]	Fe2+
fol[e]	Folate
glc_D[e]	D-glucose
gln_L[e]	L-glutamine
glu_L[e]	L-glutamate(1-)
gly[e]	Glycine
gthrd[e]	Reduced glutathione
h2o[e]	Water
h[e]	proton
hco3[e]	Bicarbonate
his_L[e]	L-histidine
ile_L[e]	L-isoleucine
inost[e]	myo-inositol
k[e]	potassium
leu_L[e]	L-leucine
lys_L[e]	L-lysinium(1+)
met_L[e]	L-methionine
na1[e]	Sodium
ncam[e]	Nicotinamide
o2[e]	O2
phe_L[e]	L-phenylalanine
pi[e]	hydrogenphosphate
pnto_R[e]	(R)-Pantothenate
pro_L[e]	L-proline
pydx[e]	Pyridoxal
pydxn[e]	Pyridoxine
ribflv[e]	Riboflavin
ser_L[e]	L-serine
so4[e]	sulfate
thm[e]	Thiamin
thr_L[e]	L-threonine
trp_L[e]	L-tryptophan
tyr_L[e]	L-tyrosine
urate[e]	Urate
urea[e]	Urea
val_L[e]	L-valine

Table S.4. Pathways that are significantly more often active in cancer and control models, respectively.

higher presence rate fraction in control	higher presence rate fraction in cancer
'Transport, extracellular'	'Blood group synthesis'
'Steroid metabolism'	'Transport, golgi apparatus'
'Exchange/demand reaction'	'Unassigned'
'Tyrosine metabolism'	'Fatty acid synthesis'
'Transport, peroxisomal'	
'Bile acid synthesis'	
'Pyrimidine catabolism'	
'Fatty acid oxidation'	
'Transport, endoplasmic reticular'	
'Phenylalanine metabolism'	
'Tryptophan metabolism'	
'Glycine, serine, alanine and threonine metabolism'	
'Transport, lysosomal'	
'Sphingolipid metabolism'	
'Urea cycle'	
'Glutamate metabolism'	
'Glycolysis/gluconeogenesis'	
'Triacylglycerol synthesis'	
'beta-Alanine metabolism'	
'N-glycan synthesis'	
'Glutathione metabolism'	

Table S.5. Essential genes. Knock-out were performed using as optimization function the production of biomass or ATP production. Enrichment test were performed using different genes lists for the different optimization function, for the case in which essential genes were pooled and for conserved essential genes. The number of essential genes in Recon 2.4 per category.

name	Recon 2.04	description
all_genes_intersect_a	0	essential for ATP in every model <0.5
all_genes_intersect_b	1	essential for biomass in every model <0.5
all_genes_union_a	34	essential for ATP in all model <0.5
all_genes_union_b	99	essential for biomass in every model <0.5
cancer_genes_intersect_a	0	essential for ATP in every cancer <0.5
cancer_genes_intersect_b	32	essential for biomass in every cancer<0.5
cancer_genes_union_a	3	essential for ATP in all cancer<0.5
cancer_genes_union_b	92	essential for biomass in all cancer<0.5
healthy_genes_intersect_a	0	essential for ATP in every healthy <0.5
healthy_genes_intersect_b	18	essential for biomass in every healthy<0.5
healthy_genes_union_a	33	essential for ATP in all healthy<0.5
healthy_genes_union_b	88	essential for biomass in all healthy<0.5
healthy_genes_intersect_a	2	essential for ATP in every healthy <0.9
healthy_genes_intersect_b	20	essential for biomass in every healthy<0.9
healthy_genes_union_a	99	essential for ATP in all healthy<0.9
healthy_genes_union_b	145	essential for biomass in all healthy<0.9
cancer_only_genes_intersect_aa	0	not essential for ATP in every healthy but essential for ATP in every cancer
cancer_only_genes_intersect_ab	29	not essential for ATP in every healthy but essential for biomass in every cancer
cancer_only_genes_intersect_bb	0	not essential for biomass in every healthy but essential for healthy in every cancer
cancer_only_genes_union_aa	1	not essential for ATP in all healthy but essential for ATP in all cancer
cancer_only_genes_union_ab	58	not essential for ATP in all healthy but essential for biomass in all cancer
cancer_only_genes_union_bb	39	not essential for biomass in all healthy but essential for biomass in all cancer

Table S.6. Overview of the websites used to find cancer drugs. As of April 2017, the listed websites provided information on currently used and approved drugs for cancer.

Name	Description
National Cancer Institute	provides general information on cancer and its treatments including a list of more than 200 approved drugs and drug combinations for cancer https://www.cancer.gov/about-cancer/treatment/drugs
SEER*Rx	an antineoplastic drug database https://seer.cancer.gov/seertools/seerrx/#
ChemoCare	cancer drugs and side effects database http://chemocare.com/chemotherapy/drug-info/default.aspx
CenterWatch	a clinical trial database https://www.centerwatch.com/drug-information/fda-approved-drugs/therapeutic-area/12/oncology
MediLexicon	a drug database http://www.medilexicon.com/drugs-list/cancer.php
Navigating Care	a chemotherapy drugs database oriented towards patients https://www.navigatingcare.com/library/all/chemotherapy_drugs

Table S.7. Complementary information on ketoconazole, naftifine, and mimosine.

Drug Name	**Origin**	**Solvent**	**Gene target**	**Current use**	**Mode of action**	**References**
Ketoconazole (M= 531.43)	synthetic imidazole-based drug	DMSO: (20 mg/mL) (warmed)	CYP51A1	antifungal	As P450 enzyme inhibitor it decreases xenobiotic metabolism	-increases intratumor drug levels and antitumor activity of fenretinide[25] and venetoclax[26] -modulation of microbial communities[27] -causes regression of advanced prostatic cancer patients by suppressing plasma androgens levels[28,29] -reduces cell proliferation of colon cancer cells[30]
Naftifine (M= 323.86)	synthetic allylamine derivative	DMSO: 5 mg/mL (warmed)	SQLE	antifungal	It inhibits squalene epoxidase, which decreases sterol-levels in fungal cell membranes	-exhibits toxicity to hematological neoplasms in vitro[31] -reduces superoxide production and polymorphonuclear leukocyte chemotaxis/endothelial adhesion[32] -inhibits squalene epoxidase[33]
Mimosine (M= 198.18)	Non-protein amino acid of Mimosoideae	DPBS + Sodium Bicarbonate (10%): 15mg/mL (warmed)	SHMT1 (protein-arginine omega-N methyl-transferase HMT1)	anti-neoplastic alanine-substituted pyridine derivative	As iron/zinc chelator it leads to the depletion of iron, which results in DNA double-strand breaks	-cell cycle inhibition of colon cancer cells[34] -cell cycle inhibition and anti-proliferative in human lung cancer cells[35] -potential role of in malignant glioma treatment,[36] regenerative dentistry,[37] and phytoremediation[38] -induces apoptosis in glioma cells via ROS and p38/JNK activation[36]

Table S.8. Short overview of the predicted drug targets and their drugs.

Drug Name	Gene target	Current use	Reference
Trimethoprim	DHFR	antibiotic	”DHFRi - dihydrofolate reductase inhibitor, a substance that can build up in cancer cells and block them from using folate. Folate is a nutrient that rapidly dividing cells need to make DNA. Blocking folate use helps keep cancer cells from growing and may kill them. Some dihydrofolate reductase inhibitors are used to treat cancer. A dihydrofolate reductase inhibitor is a type of antifolate. Also called DHFR inhibitor.” https://www.cancer.gov/publications/dictionaries/cancer-terms?cdrid=754028 “the antifolates trimethoprim and pyrimethamine are potent inhibitors of bacterial and protozoal DHFRs, respectively, but are only weak inhibitors of mammalian DHFRs”[39]
Trimethoprim	TYMS (thymidylate synthetase, TS)	antibiotic	“microRNA-612 [. . .], which is known to reduce stemness and to relieve drug resistance to cisplatin and 5-fluorouracil, possibly by targeting TYMS [via Wnt signaling] in cancer cells”[40]
Furosemide	SLCO2A1	edema and chronic renal insufficiency	“Furosemide administration reduced choline uptake in tumour lesions, especially significant in pelvic lymph node metastases.”[41] Furosemide reverses multidrug resistance status in bladder cancer cells in vitro. [42] ”The most commonly used diuretic, furosemide (Lasix®), causes the kidneys to produce more urine. As a result, the amount of free water in the body is reduced. Along with an increase in urine volume, furosemide causes loss of calcium, sodium and potassium. Furosemide is well tolerated; however, it is not free of side effects, which may include dehydration, low blood potassium and low blood sodium” http://news.cancerconnect.com/types-of-cancer/bone-cancer/hypercalcemia/ Nebulized furosemide as a novel treatment for dyspnea in terminal cancer patients[43]
Naftifine	SQLE	antifungal	“Naftifine exhibits toxicity to hematological neoplasms in vitro. [. . .] Naftifine was used in the present study since it has chemical features similar to those of other known WNT inhibitors. Materials and Methods: The anti-tumor apoptotic effect of naftifine at doses ranging from 0.1-200μM was investigated on two human and one murine lymphoma, as well as in one murine and three human myeloma cell lines”[31]
Terbinafine	SQLE	antifungal	“These findings demonstrate for the first time that TB can inhibit the proliferation of tumor cells (COLO205, HT29) in vitro and in vivo.[30–120 μM]”[44] Terbinafine inhibits KSR1 and suppresses Raf-MEK-ERK signaling in oral squamous cell carcinoma cells. [anti-neoplasia][45] Terbinafine inhibits oral squamous cell carcinoma growth through anti-cancer cell proliferation and anti-angiogenesis[46] Terbinafine inhibits endothelial cell migration through suppression of the Rho-mediated pathway[47]

Drug Name	Gene target	Current use	Reference
Tioconazole	CYP51A1	antifungal	No paper
Ketoconazole (P450 enzyme inhibitor)	CYP51A1	antifungal	"ketoconazole can be used as a pan-antagonist of NRs involved in xenobiotic metabolism (Cyp3A4) in vivo, which may lead to novel strategies that improve drug effect and tolerance"[48] P450 inhibitor ketoconazole increased the intratumor drug levels and antitumor activity of fenretinide in human neuroblastoma xenograft models [25] Effect of ketoconazole, a strong CYP3A inhibitor, on the pharmacokinetics of venetoclax, a BCL-2 inhibitor, in patients with non-Hodgkin lymphoma[26] "In the serum independent HT29-S-B6 colon cell clone, ketoconazole reduced cell proliferation and [3H]thymidine incorporation in a dose-dependent fashion, with a 50% inhibitory concentration of approximately 2.5 microM."[30]
Mimosine	SHMT1 (protein-arginine omega-N methyl-transferase HMT1)	antineoplastic alanine-substituted pyridine derivative	"Inhibition of cell cycle progression by mimosine (MIM), a reversible cell cycle blocker, reduced the percentage of migrating cells (SW480)."[34] The Chemistry and Biological Activities of Mimosine: A Review. "Interestingly, the new roles of mimosine in malignant glioma treatment, regenerative dentistry, and phytoremediation are being emerged"[38] Mimosine-induced apoptosis in C6 glioma cells requires the release of mitochondria-derived reactive oxygen species and p38, JNK activation. "Mimosine markedly inhibited proliferation and induced apoptosis of C6 glioma cells in a dose- and time-dependent manner"[36]
Orlistat	FASN (Fatty acid synthase)	obesity treatment	"[. . .] the combination of lonidamine (LND), 6-diazo-5-oxo-L-norleucine (DON) and orlistat [. . .] (triple metabolic blockade of the malignant phenotype) appears feasible and promising for [colon] cancer therapy."[49] Fatty acid synthase as a potential therapeutic target in cancer. "Early small-molecule FASN inhibitors such as cerulenin, C75 and orlistat have been shown to induce apoptosis in several cancer cell lines and to induce tumor growth delay in several cancer xenograft models but their mechanism is still not well understood. These molecules suffer from pharmacological limitations and weight loss as a side effect that prevent their development as systemic drugs. Several potent inhibitors have recently been reported that may help to unravel and exploit the full potential of FASN as a target for cancer therapy in the near future. Furthermore, novel sources of FASN inhibitors, such as green tea and dietary soy, make both dietary manipulation and chemoprevention potential alternative modes of therapy in the future."[50]
Butenafine	SQLE (cholesterol synthesis)	antifungal	No paper "SQLE promotes cancer progression in multiple types of cancer. Again, its role in colon cancer progression was undefined."[51] SQLE induces epithelial-to-mesenchymal transition by regulating of miR-133b in esophageal squamous cell carcinoma.[52] Cholesterol biosynthesis pathway as a novel mechanism of resistance to estrogen deprivation in estrogen receptor-positive breast cancer.[53]

Drug Name	Gene target	Current use	Reference
Atovaquone	DHODH (Dihydroorotate dehydrogenase), Pyrimidine biosynthesis	antimicrobial, antimalarial	Gene expression-based discovery of atovaquone as a STAT3 inhibitor and anti-cancer agent. "These findings establish atovaquone as a novel, clinically-accessible STAT3 inhibitor with evidence of anti-cancer efficacy in both animal models and humans."[54] The anti-malarial atovaquone increases radiosensitivity by alleviating tumour hypoxia. "it reduces hypoxia in FaDu and HCT116 xenografts in nude mice, and causes a significant tumour growth delay when combined with radiation"[55] Repurposing atovaquone: targeting mitochondrial complex III and OXPHOS to eradicate cancer stem cells. "atovaquone [1μM] also induces apoptosis in both CD44+/CD24low/- CSC and ALDH+ CSC populations, during exposure to anchorage-independent conditions for 12 hours."**?** Atovaquone derivatives as potent cytotoxic and apoptosis inducing agents. "Several compounds displayed significantly improved cytotoxic activities against a panel of cancer cell lines than that of atovaquone"[56]
Sertaconazole	CYP51A1	antifungal	no paper
Itraconazole	CYP51A1	antifungal	Inhibition of angiogenesis by the antifungal drug itraconazole. "Itraconazole inhibits endothelial cell cycle progression at the G1 phase in vitro and blocks vascular endothelial growth factor/basic fibroblast growth factor-dependent angiogenesis in vivo.[57] Itraconazole inhibits angiogenesis and tumor growth in non-small cell lung cancer. "itraconazole has potent and selective inhibitory activity against multiple key aspects of tumor-associated angiogenesis in vitro and *in vivo*"[58] Recent advances in drug repurposing for the discovery of new anticancer drugs. "[(Nacev et al. 2011)] showed that itraconazole inhibited cholesterol trafficking in human endothelial cells, leading to inhibition of mammalian target of rapamycin (mTOR) and vascular endothelial growth factor receptor type 2 (VEGFR2) signaling pathways that are critical for endothelial cell proliferation and angiogenesis"[59]
Lactic Acid	SLCO2A1		"increasing evidence that cancers can escape immune destruction by suppressing the anti-cancer immune response through maintaining a relatively low pH in their micro-environment. Tumours achieve this by regulating lactic acid secretion via modification of glucose/glutamine metabolisms."[60]

Drug Name	Gene target	Current use	Reference
Icatibant (bradykinin receptor antagonist)	SLCO2A1 (solute carrier organic anion transporter family member 2A1)	peptidomimetic drug, hereditary angioedema	"the oral treatment significantly inhibited the development of [Dextran sulfate sodium-induced] colitis [in mice] that was observed histopathologically."[61] Influence of Genetic Polymorphisms in Prostaglandin E2 Pathway (COX-2/HPGD/SLCO2A1/ABCC4) on the Risk for Colorectal Adenoma Development and Recurrence after Polypectomy.[62] Prostaglandin transporter, SLCO2A1, mediates the invasion and apoptosis of lung cancer cells via PI3K/AKT/mTOR pathway.[63] Mechanisms involved in kinin-induced glioma cells proliferation: the role of ERK1/2 and PI3K/Akt pathways.[64] Identification of bradykinin receptors in clinical cancer specimens and murine tumor tissues.[65]
Canagliflozin (sodium glucose cotransporter type 2 (SGLT2) inhibitor)	SLC5A1	anti-diabetic drugs	"canagliflozin is able to reduce tumor growth and increase the necrosis in the tumor center."[66] "Canagliflozin, but not Dapagliflozin, potently suppress proliferation and clonogenic survival of cancer cells alone and in combination with cytotoxic therapies."[67] "Relationship between SGLT2 inhibition and cancer formation is still inconclusive and studies with larger sample size, longer exposure duration, and different ethnicities are warranted."[68]
Sodium fluoride	MT-CO1	prevent cavities	"population-based-studies strongly suggest that chronic fluoride ingestion is a possible cause of uterine cancer and bladder cancer; there may be a link with osteosarcoma—highlighted as an area where there is evidence of problems requiring further research"[69]

Table S.9. Model numerics for models reconstructed with the INIT algorithm. Overview on the number of reaction, metabolites, and genes of the 26 model reconstructed with INIT. Model were constructed using the consistent Recon 2 model and weights for each reaction as input.

Tissue	Number of reactions	Number of metabolites	Number of genes
Input model (consistent Recon 2.04)	5317	2960	1913
BRCA cancer	3042	2079	1431
COAD cancer	3472	2345	1478
HNSC cancer	3345	2278	1428
KICH cancer	3229	2213	1580
KIRC cancer	3336	2294	1527
KIRP cancer	3239	2216	1556
LIHC cancer	3633	2431	1567
LUAD cancer	3242	2206	1474
LUSC cancer	3335	2270	1537
PRAD cancer	3431	2327	1450
STAD cancer	3352	2267	1462
THCA cancer	3181	2186	1552
UCEC cancer	3170	2152	1428
BRCA control	3278	2236	1486
COAD control	3618	2438	1645
HNSC control	3334	2282	1402
KICH control	3503	2384	1582
KIRC control	3460	2345	1613
KIRP control	3447	2340	1581
LIHC control	3900	2537	1750
LUAD control	3411	2324	1554
LUSC control	3386	2284	1534
PRAD control	3362	2297	1547
STAD control	3240	2220	1430
THCA control	3258	2220	1611
UCEC control	3232	2213	1495

References

[1] Horng-Dar W, Chiou-Hwa Y, Hsiao YC, Yu-Ting C. Method for early diagnosis of liver cancer and prediction of metastasis. Google Patents; 2014. US Patent 8,628,920.

[2] Pacheco MP, John E, Kaoma T, Heinäniemi M, Nicot N, Vallar L, et al. Integrated metabolic modelling reveals cell-type specific epigenetic control points of the macrophage metabolic network. BMC genomics. 2015;16(1):809.

[3] Fan Y, Xi L, Hughes DS, Zhang J, Zhang J, Futreal PA, et al. MuSE: accounting for tumor heterogeneity using a sample-specific error model improves sensitivity and specificity in mutation calling from sequencing data. Genome Biology. 2016;17(1):178.

[4] Cibulskis K, Lawrence MS, Carter SL, Sivachenko A, Jaffe D, Sougnez C, et al. Sensitive detection of somatic point mutations in impure and heterogeneous cancer samples. Nature biotechnology. 2013;31(3):213–219.

[5] Simola DF, Kim J. Sniper: improved SNP discovery by multiply mapping deep sequenced reads. Genome biology. 2011;12(6):R55.

[6] Koboldt DC, Zhang Q, Larson DE, Shen D, McLellan MD, Lin L, et al. VarScan 2: somatic mutation and copy number alteration discovery in cancer by exome sequencing. Genome research. 2012;22(3):568–576.

[7] Cui R, Kamatani Y, Takahashi A, Usami M, Hosono N, Kawaguchi T, et al. Functional variants in ADH1B and ALDH2 coupled with alcohol and smoking synergistically enhance esophageal cancer risk. Gastroenterology. 2009;137(5):1768–1775.

[8] Yang SJ, Yokoyama A, Yokoyama T, Huang YC, Wu SY, Shao Y, et al. Relationship between genetic polymorphisms of ALDH2 and ADH1B and esophageal cancer risk: a meta-analysis. World J Gastroenterol. 2010;16(33):4210–20.

[9] Masaoka H, Ito H, Soga N, Hosono S, Oze I, Watanabe M, et al. Aldehyde dehydrogenase 2 (ALDH2) and alcohol dehydrogenase 1B (ADH1B) polymorphisms exacerbate bladder cancer risk associated with alcohol drinking: gene–environment interaction. Carcinogenesis. 2016;37(6):583–588.

[10] Chang JS, Straif K, Guha N. The role of alcohol dehydrogenase genes in head and neck cancers: a systematic review and meta-analysis of ADH1B and ADH1C. Mutagenesis. 2012;27(3):275–286.

[11] Cai Q, Wu J, Cai Q, Chen EZ, Jiang ZY. Association between Glu504Lys polymorphism of ALDH2 gene and cancer risk: a meta-analysis. PloS one. 2015;10(2):e0117173.

[12] Zhang J, Tsoi H, Li X, Wang H, Gao J, Wang K, et al. Carbonic anhydrase IV inhibits colon cancer development by inhibiting the Wnt signalling pathway through targeting the WTAP–WT1–TBL1 axis. Gut. 2015;p. gutjnl–2014.

[13] Chen B, Hu KW, Zhang JW, Wei ZJ, Meng XL, Xiong MM. A critical Analysis of the Relationship Between Aldehyde dehydrogenases-2 Glu487Lys Polymorphism and Colorectal Cancer Susceptibility. Pathology & Oncology Research. 2015;21(3):727–733.

[14] Li R, Zhao Z, Sun M, Luo J, Xiao Y. ALDH2 gene polymorphism in different types of cancers and its clinical significance. Life sciences. 2016;147:59–66.

[15] Lin CW, Shen SC, Hou WC, Yang LY, Chen YC. Heme oxygenase-1 inhibits breast cancer invasion via suppressing the expression of matrix metalloproteinase-9. Molecular cancer therapeutics. 2008;7(5):1195–1206.

[16] Varki A, Kannagi R, Toole BP. Glycosylation changes in cancer. 2009;.

[17] Scheerger, Zempleni. Expression of oncogenes depends on biotin in human small cell lung cancer cells NCI-H69. International journal for vitamin and nutrition research. 2003;73(6):461–467.

[18] Jariwala U, Prescott J, Jia L, Barski A, Pregizer S, Cogan JP, et al. Identification of novel androgen receptor target genes in prostate cancer. Molecular cancer. 2007;6(1):1.

[19] Possemato R, Marks KM, Shaul YD, Pacold ME, Kim D, Birsoy K, et al. Functional genomics reveal that the serine synthesis pathway is essential in breast cancer. Nature. 2011;476(7360):346–350.

[20] Agren R, Bordel S, Mardinoglu A, Pornputtapong N, Nookaew I, Nielsen J. Reconstruction of genome-scale active metabolic networks for 69 human cell types and 16 cancer types using INIT. PLoS Comput Biol. 2012;8(5):e1002518.

[21] Wang T, Birsoy K, Hughes NW, Krupczak KM, Post Y, Wei JJ, et al. Identification and characterization of essential genes in the human genome. Science (New York, NY). 2015 nov;350(6264):1096–101. Available from: http://science.sciencemag.org/content/350/6264/1096.short{%}5Cnpapers3://publication/doi/10.1126/science.aac7557http://www.sciencemag.org/cgi/doi/10.1126/science.aac7041http://arxiv.org/abs/1011.1669http://dx.doi.org/10.1088/1751-8113/44/8/085201http://www.ncbi.nlm.nih.gov/pubmed/26472758http://www.pubmedcentral.nih.gov/articlerender.fcgi?artid=PMC4662922.

[22] Hart T, Chandrashekhar M, Aregger M, Steinhart Z, Brown KR, MacLeod G, et al. High-resolution CRISPR screens reveal fitness genes and genotype-specific cancer liabilities. Cell. 2015;163(6):1515–1526.

[23] Blomen VA, Majek P, Jae LT, Bigenzahn JW, Nieuwenhuis J, Staring J, et al. Gene essentiality and synthetic lethality in haploid human cells. Science. 2015 nov;350(6264):1092–1096. Available from: http://www.sciencemag.org/cgi/doi/10.1126/science.aac7557{%}5Cnhttp://www.ncbi.nlm.nih.gov/pubmed/26472760http://www.sciencemag.org/cgi/doi/10.1126/science.aac7557.

[24] Hart T, Komori HK, LaMere S, Podshivalova K, Salomon DR. Finding the active genes in deep RNA-seq gene expression studies. BMC Genomics. 2013;14(1):1–7. Available from: http://dx.doi.org/10.1186/1471-2164-14-778.

[25] Lopez-Barcons L, Maurer BJ, Kang MH, Reynolds CP. P450 inhibitor ketoconazole increased the intratumor drug levels and antitumor activity of fenretinide in human neuroblastoma xenograft models. International journal of cancer. 2017;141(2):405–413.

[26] Agarwal SK, Salem AH, Danilov AV, Hu B, Puvvada S, Gutierrez M, et al. Effect of ketoconazole, a strong CYP3A inhibitor, on the pharmacokinetics of venetoclax, a BCL-2 inhibitor, in patients with non-Hodgkin lymphoma. British journal of clinical pharmacology. 2017;83(4):846–854.

[27] Van Cutsem J, Van Gerven F, Cauwenbergh G, Odds F, Janssen PA. The antiinflammatory effects of ketoconazole: A comparative study with hydrocortisone acetate in a model using living and killed Staphylococcus aureus on the skin of guinea pigs. Journal of the American Academy of Dermatology. 1991;25(2):257–261.

[28] Trump DL, Havlin KH, Messing EM, Cummings KB, Lange PH, Jordan VC. High-dose ketoconazole in advanced hormone-refractory prostate cancer: endocrinologic and clinical effects. Journal of Clinical Oncology. 1989;7(8):1093–1098.

[29] Harris KA, Weinberg V, Bok RA, Kakefuda M, Small EJ. Low dose ketoconazole with replacement doses of hydrocortisone in patients with progressive androgen independent prostate cancer. The Journal of urology. 2002;168(2):542–545.

[30] Forgue-Lafitte ME, Coudray AM, Fagot D, Mester J. Effects of ketoconazole on the proliferation and cell cycle of human cancer cell lines. Cancer research. 1992;52(24):6827–6831.

[31] SCHMEEL LC, SCHMEEL FC, BLAUM-FEDER S, SCHMIDT-WOLF IG. In vitro efficacy of naftifine against lymphoma and multiple myeloma. Anticancer research. 2015;35(11):5921–5926.

[32] Gupta AK, Ryder JE, Cooper EA. Naftifine: a review. Journal of cutaneous medicine and surgery. 2008;12(2):51–58.

[33] Ryder NS. Specific inhibition of fungal sterol biosynthesis by SF 86-327, a new allylamine antimycotic agent. Antimicrobial agents and chemotherapy. 1985;27(2):252–256.

[34] Kubens BS, Niggemann B, Zänker KS. Prevention of entrance into G2 cell cycle phase by mimosine decreases locomotion of cells from the tumor cell line SW480. Cancer letters. 2001;162:S39–S47.

[35] Chang H, Weng C, Yen M, Chuang L, Hung W. Modulation of cell cycle regulatory protein expression and suppression of tumor growth by mimosine in nude mice. International journal of oncology. 2000;17(4):659–724.

[36] Qiao S, Murakami K, Zhao Q, Wang B, Seo H, Yamashita H, et al. Mimosine-induced apoptosis in C6 glioma cells requires the release of mitochondria-derived reactive oxygen species and p38, JNK activation. Neurochemical research. 2012;37(2):417–427.

[37] Agis H, Watzek G, Gruber R. Prolyl hydroxylase inhibitors increase the production of vascular endothelial growth factor by periodontal fibroblasts. Journal of periodontal research. 2012;47(2):165–173.

[38] Nguyen BCQ, Tawata S. The Chemistry and Biological Activities of Mimosine: A Review. Phytotherapy Research. 2016;30(8):1230–1242.

[39] Schweitzer BI, Dicker AP, Bertino JR. Dihydrofolate reductase as a therapeutic target. The FASEB Journal. 1990;4(8):2441–2452.

[40] Tang J, Tao ZH, Wen D, Wan JL, Liu DL, Zhang S, et al. MiR-612 suppresses the stemness of liver cancer via Wnt/β-catenin signaling. Biochemical and biophysical research communications. 2014;447(1):210–215.

[41] Rischke HC, Beck T, Vach W, Wieser G, Grosu AL, Schultze-Seemann W, et al. Furosemide diminishes 18 F-fluoroethylcholine uptake in prostate cancer in vivo. European journal of nuclear medicine and molecular imaging. 2014;41(11):2074–2082.

[42] Speers AG, Lwaleed BA, Featherstone JM, Sallis BJ, Cooper AJ. Furosemide reverses multidrug resistance status in bladder cancer cells in vitro. Journal of clinical pathology. 2006;59(9):912–915.

[43] Shimoyama N, Shimoyama M. Nebulized furosemide as a novel treatment for dyspnea in terminal cancer patients. Journal of pain and symptom management. 2002;23(1):73–76.

[44] Lee WS, Chen RJ, Wang YJ, Tseng H, Jeng JH, Lin SY, et al. In vitro and in vivo studies of the anticancer action of terbinafine in human cancer cell lines: G0/G1 p53-associated cell cycle arrest. International journal of cancer. 2003;106(1):125–137.

[45] Li B, Lu L, Zhong M, Tan X, Liu C, Guo Y, et al. Terbinafine inhibits KSR1 and suppresses Raf-MEK-ERK signaling in oral squamous cell carcinoma cells. Neoplasma. 2013;60(4):406–412.

[46] Chien MH, Lee TS, Kao C, Yang SF, Lee WS. Terbinafine inhibits oral squamous cell carcinoma growth through anti-cancer cell proliferation and anti-angiogenesis. Molecular carcinogenesis. 2012;51(5):389–399.

[47] Ho PY, Zhong WB, Ho YS, Lee WS. Terbinafine inhibits endothelial cell migration through suppression of the Rho-mediated pathway. Molecular cancer therapeutics. 2006;5(12):3130–3138.

[48] Huang H, Wang H, Sinz M, Zoeckler M, Staudinger J, Redinbo M, et al. Inhibition of drug metabolism by blocking the activation of nuclear receptors by ketoconazole. Oncogene. 2007;26(2):258.

[49] Cervantes-Madrid D, Dominguez-Gomez G, Gonzalez-Fierro A, Perez-Cardenas E, Taja-Chayeb L, Trejo-Becerril C, et al. Feasibility and antitumor efficacy in vivo, of simultaneously targeting glycolysis, glutaminolysis and fatty acid synthesis using lonidamine, 6-diazo-5-oxo-L-norleucine and orlistat in colon cancer. Oncology letters. 2017;13(3):1905–1910.

[50] Flavin R, Peluso S, Nguyen PL, Loda M. Fatty acid synthase as a potential therapeutic target in cancer. Future oncology. 2010;6(4):551–562.

[51] Yuen HF, McCrudden CM, Huang YH, Tham JM, Zhang X, Zeng Q, et al. TAZ expression as a prognostic indicator in colorectal cancer. PloS one. 2013;8(1):e54211.

[52] Qin Y, Zhang Y, Tang Q, Jin L, Chen Y. SQLE induces epithelial-to-mesenchymal transition by regulating of miR-133b in esophageal squamous cell carcinoma. Acta biochimica et biophysica Sinica. 2017;49(2):138–148.

[53] Simigdala N, Gao Q, Pancholi S, Roberg-Larsen H, Zvelebil M, Ribas R, et al. Cholesterol biosynthesis pathway as a novel mechanism of resistance to estrogen deprivation in estrogen receptor-positive breast cancer. Breast Cancer Research. 2016;18(1):58.

[54] Xiang M, Kim H, Ho VT, Walker SR, Bar-Natan M, Liu S, et al. Gene expression-based discovery of atovaquone as a STAT3 inhibitor and anti-cancer agent. Blood. 2016;p. blood–2015.

[55] Ashton TM, Fokas E, Kunz-Schughart LA, Folkes LK, Anbalagan S, Huether M, et al. The anti-malarial atovaquone increases radiosensitivity by alleviating tumour hypoxia. Nature communications. 2016;7:12308.

[56] Zhou J, Duan L, Chen H, Ren X, Zhang Z, Zhou F, et al. Atovaquone derivatives as potent cytotoxic and apoptosis inducing agents. Bioorganic & medicinal chemistry letters. 2009;19(17):5091–5094.

[57] Chong CR, Xu J, Lu J, Bhat S, Sullivan Jr DJ, Liu JO. Inhibition of angiogenesis by the antifungal drug itraconazole. ACS chemical biology. 2007;2(4):263–270.

[58] Aftab BT, Dobromilskaya I, Liu JO, Rudin CM. Itraconazole inhibits angiogenesis and tumor growth in non–small cell lung cancer. Cancer research. 2011;.

[59] Shim JS, Liu JO. Recent advances in drug repositioning for the discovery of new anticancer drugs. International journal of biological sciences. 2014;10(7):654.

[60] Choi SYC, Collins CC, Gout PW, Wang Y. Cancer-generated lactic acid: a regulatory, immunosuppressive metabolite? The Journal of pathology. 2013;230(4):350–355.

[61] Arai Y, Takanashi H, Kitagawa H, Wirth KJ, Okayasu I. Effect of icatibant, a bradykinin B2 receptor antagonist, on the development of experimental ulcerative colitis in mice. Digestive diseases and sciences. 1999;44(4):845–851.

[62] Pereira C, Queirós S, Galaghar A, Sousa H, Marcos-Pinto R, Pimentel-Nunes P, et al. Influence of Genetic Polymorphisms in Prostaglandin E2 Pathway (COX-2/HPGD/SLCO2A1/ABCC4) on the Risk for Colorectal Adenoma Development and Recurrence after Polypectomy. Clinical and translational gastroenterology. 2016;7(9):e191.

[63] Zhu Q, Liang X, Dai J, Guan X. Prostaglandin transporter, SLCO2A1, mediates the invasion and apoptosis of lung cancer cells via PI3K/AKT/mTOR pathway. International journal of clinical and experimental pathology. 2015;8(8):9175.

[64] Nicoletti NF, Erig TC, Zanin RF, Pereira TCB, Bogo MR, Campos MM, et al. Mechanisms involved in kinin-induced glioma cells proliferation: the role of ERK1/2 and PI3K/Akt pathways. Journal of neuro-oncology. 2014;120(2):235–244.

[65] Wu J, Akaike T, Hayashida K, Miyamoto Y, Nakagawa T, Miyakawa K, et al. Identification of bradykinin receptors in clinical cancer specimens and murine tumor tissues. International journal of cancer. 2002;98(1):29–35.

[66] Scafoglio C, Hirayama BA, Kepe V, Liu J, Ghezzi C, Satyamurthy N, et al. Functional expression of sodium-glucose transporters in cancer. Proceedings of the National Academy of Sciences. 2015;112(30):E4111–E4119.

[67] Villani LA, Smith BK, Marcinko K, Ford RJ, Broadfield LA, Green AE, et al. The diabetes medication Canagliflozin reduces cancer cell proliferation by inhibiting mitochondrial complex-I supported respiration. Molecular metabolism. 2016;5(10):1048–1056.

[68] Lin HW, Tseng CH. A review on the relationship between SGLT2 inhibitors and cancer. International journal of endocrinology. 2014;2014.

[69] Peckham S, Awofeso N. Water fluoridation: a critical review of the physiological effects of ingested fluoride as a public health intervention. The Scientific World Journal. 2014;2014.